DEVELOPMENT OF BEAM SCHEDULING ALGORITHM FOR FREQUENCY DIVERSE ARRAY

A THESIS SUBMITTED TO
THE GRADUATE SCHOOL OF NATURAL AND APPLIED SCIENCES
OF
MIDDLE EAST TECHNICAL UNIVERSITY

BY

RAMAZAN ÇETİNER

IN PARTIAL FULFILLMENT OF THE REQUIREMENTS
FOR
THE DEGREE OF MASTER OF SCIENCE
IN
ELECTRICAL AND ELECTRONICS ENGINEERING

FEBRUARY 2015

Approval of the thesis:

DEVELOPMENT OF BEAM SCHEDULING ALGORITHM FOR FREQUENCY DIVERSE ARRAY

submitted by **RAMAZAN ÇETİNER** in partial fulfillment of the requirements for the degree of **Master of Science in Electrical and Electronics Engineering Department, Middle East Technical University** by,

Prof. Dr. Gülbin Dural Ünver
Dean, Graduate School of **Natural and Applied Sciences** _____

Prof. Dr. Gönül Turhan Sayan
Head of Department, **Electrical and Electronics Engineering** _____

Prof. Dr. Şimşek Demir
Supervisor, **Electrical and Electronics Engineering Dept., METU** _____

Examining Committee Members:

Prof. Dr. Canan Toker
Electrical and Electronics Engineering Dept., METU _____

Prof. Dr. Şimşek Demir
Electrical and Electronics Engineering Dept., METU _____

Prof. Dr. Altunkan Hızal
Electrical and Electronics Engineering Dept., METU _____

Prof. Dr. Sencer Koç
Electrical and Electronics Engineering Dept., METU _____

Dr. Taylan Eker
ASELSAN Inc. _____

Date: **27/02/2015**

I hereby declare that all information in this document has been obtained and presented in accordance with academic rules and ethical conduct. I also declare that, as required by these rules and conduct, I have fully cited and referenced all material and results that are not original to this work.

Name, Last name : Ramazan ÇETİNER

Signature :

ABSTRACT

DEVELOPMENT OF BEAM SCHEDULING ALGORITHM FOR FREQUENCY DIVERSE ARRAY

Çetiner, Ramazan
M.S., Department of Electrical and Electronics Engineering
Supervisor: Prof. Dr. Şimşek Demir
February 2015, 81 pages

Electronic scanning is the most desirable feature of radar systems. With electronic scanning, it is possible to steer the main beam of an array antenna instantaneously into a desired direction where no mechanical mechanism is involved in the scanning process. Electronic scanning methods including phase scanning, time delay scanning, and frequency scanning have been used in various radar applications; however new and cheaper scanning methods are still being investigated. It is the purpose of this thesis to investigate an array configuration called frequency diverse array (FDA), which gives rise to range, time, and angle dependent scanning without using phase shifters. In this study, mathematical analysis of FDA are made and DDS based FDA beamforming network is designed. Also FDA implementation is realized with this network. Justification of the mathematical derivations is made by the results of the measurements with the implemented structure. Besides, simulations and measurements of the array with various amplitude tapering coefficients are performed. The drawbacks are also reported during the study, which will be useful for future studies on the subject.

Keywords: DDS, FDA, Frequency Diverse Array

ÖZ

AYRIK FREKANSLI DİZİLERİ İÇİN HUZME YÖNLENDİRME ALGORİTMASI

Çetiner, Ramazan
Yüksek Lisans, Elektrik ve Elektronik Mühendisliği Bölümü
Tez Yöneticisi: Prof. Dr. Şimşek Demir
Şubat 2015, 81 sayfa

Elektronik tarama yeteneği modern radar sistemlerinin en önemli özelliklerindendir. Bu özellik sayesinde tarama esnasında herhangi bir mekanik mekanizmaya ihtiyaç duymadan anten huzmesinin istenilen yöne bakmasına imkân sağlanmaktadır. Günümüzde radar uygulamalarında faz tarama, zaman gecikmeli tarama, frekans tarama gibi elektronik tarama yöntemleri kullanılmaktadır. Yeni ve daha ucuz elektronik tarama yöntemleri için araştırmalar devam etmektedir. Bu tezin amacı zaman, faz kaydırıcı kullanmadan zaman, açı ve menzil bağımlı tarama yapabilen Ayrık Frekans Dizisini (AFD) incelemektir.

Bu çalışmada Ayrık Frekans Dizilerinin matematiksel analizi yapılmıştır. Bunun yanı sıra DSS (Direk Sayısal Sentez) tabanlı bir huzme yönlendirme ağı tasarlanmıştır. Tasarlanan bu yapı ile Ayrık Frekans Dizisi gerçekleştirilmiştir. Çeşitli genlik dağılımları için Ayrık Frekans Dizisinin benzetimleri ve ölçümleri gerçekleştirilmiştir. Çalışma esnasında karşılaşılan sorunlar AFD konusunda gelecekte yapılacak çalışmalara ışık tutması için raporlanmıştır.

Anahtar Kelimeler: DSS, AFD, Ayrık Frekanslı Dizi

To my family

ACKNOWLEDGEMENTS

I would like to express my deepest sense of gratitude to my supervisor Prof. Dr. Şimşek Demir for his guidance and invaluable ideas.

I am deeply grateful to ASELSAN Inc. for providing tools and other facilities throughout this study.

I am so grateful to Dr. Taylan Eker, Muharrem Keskin, for their valuable efforts in mathematical developments and in implementation and measurement recommendations.

I want to express my special thanks to Abdülkerim Altuntaş for his support during this study.

I would also like to express my profound appreciation to my family for their continuous support.

TABLE OF CONTENTS

LIST OF TABLES

TABLES

LIST OF FIGURES

FIGURES

LIST OF ABBREVIATIONS

AESA	:	Active Electronic Scanned Array
MSA	:	Mechanically Steered Antenna
TWTs	:	Travelling Wave Tubes
FDA	:	Frequency Diverse Array
AF	:	Array Factor
AM	:	Amplitude Modulation
DDS	:	Direct Digital Synthesis
FFT	:	Fast Fourier Transform
MTT	:	Multi Target Indicator
PLL	:	Phase Locked Loop
PPA	:	Peak Power Analyzer
SA	:	Spectrum Analyzer
SMA	:	Sub-Miniature Assembly
BNC	:	(Bayonet Neill–Concelman) connector

CHAPTER 1

INTRODUCTION

1.1. Background

An important feature of radar systems is an active electronic beam scanning that permits the main antenna beam to be steered. There are no time lags and inertia in electronic scanning methods to direct the main beam instantaneously. Active electronically scanned array (AESA) have many advantages rather than Mechanically Scanned Array (MSA). The advantages of electronic scanning include flexible beam pointing, increased data rates, avoidance of mechanical errors, increased flexibility of multi-mode operation, automatic multi-target tracking and multiple tasking [17].

A great deal of effort has been devoted to the investigation of the methods for electronic scanning of antenna systems. Frequency variation, phase shift scan (using ferrites, travelling wave tubes (TWTs), delay lines, etc.), and in a minor way, the idea of space time equivalence are techniques which have been studied on in this connection [1].

The technique for beam steering, namely Frequency Diverse Array is researched in this thesis. FDA can be defined as an array antenna for which the frequency of each element in the array can be controlled separately to steer the main beam. This concept depends on the time domain relations of each frequency component in the far field. The beam can be scanned in space periodically by applying step frequency difference between each element in array [2].Periodicity

properties of beam steering are based on the frequency difference between antenna array elements and the inter-element distance.

Unlike conventional phased arrays, a small frequency increment rather than a phase increment, is applied across the elements. It is shown that a small frequency difference across the elements generates a beam pattern whose main beam direction is a periodic function of time and range [3]. FDA is different from the conventional phased array, whose array factor is independent of range and time.

The mathematical derivations of FDA concept is performed by using basic antenna theory concepts. A basic structure was implemented and several measurements were performed in this study. Remarkable results and discussions with graphical images are presented in this thesis. MATLAB is used extensively for simulations.

1.2. Research Aims

The main purpose of this thesis is to investigate frequency diversity in electronically scanned array. Steps in the research are summarized below:

1) Examine the background of the notion of an antenna array and investigate the mathematical model of conventional phased arrays.
2) Derive the mathematical expressions of FDA using basic antenna theory and identify physical parameters to determine its radiation behavior.
3) Analyze the array factor of FDA and perform a parametric study on FDA's array factor.
4) Create the simulation to demonstrate the performance of frequency diverse signals in an 8-element array
5) Design the DDS based FDA beamforming network which produces the required frequency diverse signals. Several measurements are performed to verify the FDA concept by using this network.

1.3. Thesis Layout

In Chapter 2, a review of antenna array fundamentals is given on which the theory of FDA is based. The basic concepts such as the array factor and beam steering of the conventional phased array are demonstrated. In addition, the theory of operation for frequency scanning compared to the conventional phased array.

Chapter 3 presents the theory of FDA in details, focusing on the array factor of FDA. Related previous works on FDA is also given in this chapter. To verify the FDA concept, several simulations are presented and by means of these simulations, the key concepts in FDA are explained.

Chapter 4 describes the hardware implementation of FDA. A DDS based design of FDA beamforming network is presented. Several experiments on the FDA concept are performed by using this network. In addition, it is shown that the results of these experiments are in excellent agreement with the simulation results presented in Chapter 3.

Brief conclusions of the research and future works are finally presented in Chapter 5.

CHAPTER 2

ANTENNA ARRAY THEORY

In this chapter, the basic theory underlining the beam formation in array antennas is explained. This provides the necessary information to analyze the frequency diversity concepts in Chapter 3.

2.1. Antenna Arrays

In order to generate a high-gain directional radiation pattern, a lot of electrically small, low-gain antennas can be interconnected and arranged in space [4]. This type of configuration is known as an array antenna, or basically an array. Thanks to arrays, the main beam is capable of electronic scanning. It is possible to scan the radiation pattern through space by altering the phase of the exciting currents in each antenna element of the array. Then the array is called a phased array.

Phased array antennas allow for many advantages over conventional mechanically scanned antennas. By electronically positioning the beam, phased array antennas allow for quick beam steering without the hindrance of vibration or overshoot. The other advantages of phased array antennas are rapid and flexible scan without moving parts, multi-target tracking (MTT), the ability to form multiple simultaneous beams [5].

The phased array fundamentally relies upon the principle of the interferometer, where the interference pattern produced by two signals is utilized to obtain information about phase, frequency, beam travelling direction and time delay.

The interferometer provides the first approach to spatial diversity for forming and analysis of signals. The main lobe of the interference pattern can be steered by phase shifting.

The main beam of the antenna array can be steered by applying a linear phase shift on the signal received or transmitted at each array element. In addition, by varying the frequency of the signal, the electrical spacing between elements can be altered resulting in a change in phase progression across the elements. This causes the antenna beam to scan as frequency varies, which limits the effective bandwidth of the array [5]. The aperture scanning effect can be mitigated through the use of true time delay [6], [7]. In true time delay, the time of propagation for the paths of all radiating elements is made to be equal, causing all signals to add in phase for every frequency component in the waveform. However, this is costly to implement at the element level, so that true time delay is usually implemented on a sub-array basis [8], [9]. But, more recent advances in direct digital synthesis of the local oscillator at each element make true time delay at the element level more practical. Furthermore, direct digital synthesis at the element level enables the concept of the frequency diverse array. This may allow the compensation of frequency scan by the deliberate and progressive change in frequency between elements.

In this thesis, only linear arrays which have the same antenna elements are taken into consideration. It is possible to extend the frequency diverse array (FDA) concepts developed for linear arrays to other array configurations.

In the far-field region, the electric field from a radiating antenna element can be referred to as the multiplication of two functions. The first function is the spherical propagation factor $\frac{e^{-jkR}}{R}$, which depends on the range, and the second function is $f_e(\theta,\phi)$, which is a normalized function that accounts for the directional dependence of the element's electric field [10].

The principle of the phased array at the far-field is shown in Figure 2.1. The elements of the array are uniformly-spaced with a separation distance *d.*

The electric fields in the far zone of the array elements can be represented as

$$E_n = a_n e^{j\psi_n} \frac{e^{-jkR_n}}{R_n} f_e(\theta, \varphi) \tag{2.1}$$

where the a_n's are the amplitude excitation coefficients of the array elements and ψ_n is the phase distribution of the array. The angle theta is the angle from the normal with respect to the axis of the array (i.e., the *z*-axis in Figure 2.1)

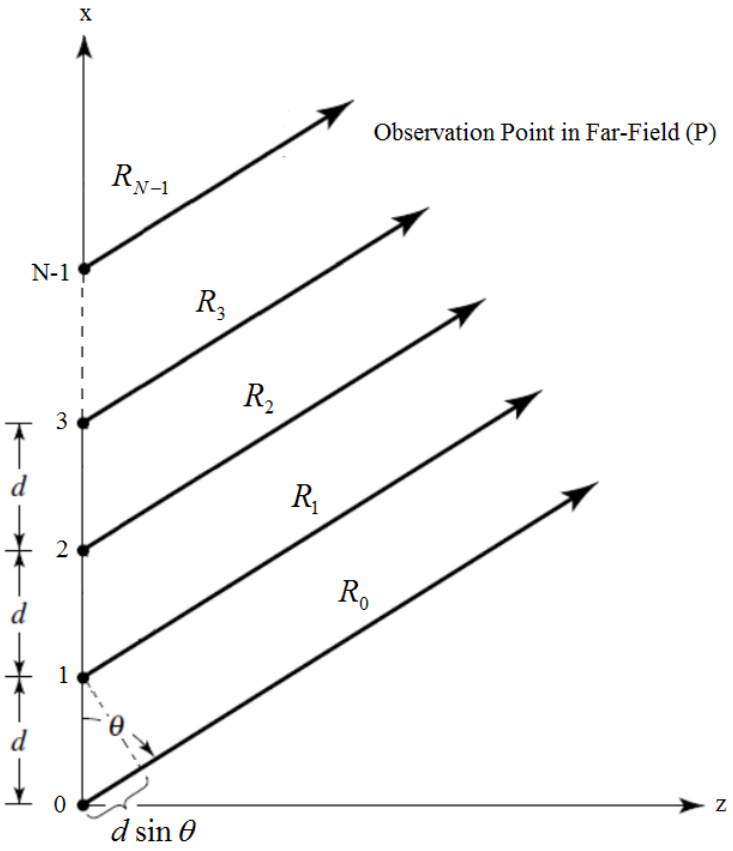

Figure 2.1: The Far field geometry of N-Element array

Only far field region is often considered in many radar applications. Therefore, some approximations can be applied [11]. The magnitude excitation of the

array elements are assumed to be equal and distances for each antenna element can be approximated by $R_n \approx R_0$.

The slight difference in the distances cannot be neglected for the exponential term, because it can generate significant phase shifts. The far field phase variations of e^{-jkR_n} term can be approximated by

$$R_n \approx R_0 - nd\sin\theta \tag{2.2}$$

Using Equations (2.1) and (2.2), the sum of all electric fields from N individual antenna elements at a far-field observation point *P* reduces to

$$E_n = f_e(\theta,\varphi)\left(\frac{e^{-jkR_0}}{R_0}\right)\sum_{n=0}^{N-1} a_n e^{j\psi_n} e^{jnkd\sin\theta} \tag{2.3}$$

The array factor AF is given by

$$AF = \sum_{n=0}^{N-1} a_n e^{j\psi_n} e^{jnkd\sin\theta} \tag{2.4}$$

The array factor AF is independent of the antenna element type. We assume that all of the elements are identical. Therefore, isotropic radiators may be utilized in the derivation of the array factor. The array factor is a function of the physical configuration of the array and the excitation (amplitude, phase) of the elements [10].

The array factor depends on the number of elements, their geometrical arrangement, and their relative amplitudes and phases. The side-lobe levels can be controlled by changing the amplitude distribution of the array given by the coefficients a_n [11]. The magnitude coefficients of the array elements are assumed to be equal so,

$$a_0 = a_1 = a_2 = ... = a_{N-1} \tag{2.5}$$

The phase distribution of the array is given by the phases ψ_n. The phase can be controlled to steer the antenna beam. The element phases are assumed to be equal, and can be set to zero $\psi_n = 0$. Hence, the array factor can be written as,

$$AF = a_0 \sum_{n=0}^{N-1} e^{jnkd\sin\theta} = a_0 \sum_{n=0}^{N-1} e^{jn\gamma} \tag{2.6}$$

where $\gamma = kd\sin(\theta)$. Equation (2.6) is a geometric series that can be expressed in compact form

$$AF = a_0 \frac{\sin(N\gamma/2)}{\sin(\gamma/2)} e^{j(N-1)\gamma/2} \tag{2.7}$$

If the phase reference point of the array element located at the origin, the phase term $e^{j(N-1)\gamma/2}$ can be neglected [11]. Therefore, the array factor of (2.7) reduces to

$$AF = a_0 \frac{\sin(N\gamma/2)}{\sin(\gamma/2)} \tag{2.8}$$

The maximum value of array factor is equal to Na_0 when γ is equal to zero. The array factor may be normalized so that the maximum value for any value of N is unity [11]. Equation (2.8) is written in the normalized form as,

$$\left|AF_{norm}\right| = \left|\frac{\sin(N\gamma/2)}{N\sin(\gamma/2)}\right| \tag{2.9}$$

The broadside array factor of an 8-element array with element spacing of $\frac{\lambda}{2}$ given in (2.9) is shown in Figure 2.2. It illustrates that if the array is uniformly fed with identical current amplitudes and no phase shift across the elements of the array is applied, the main beam points in the broadside direction $\theta = 0°$ [11].

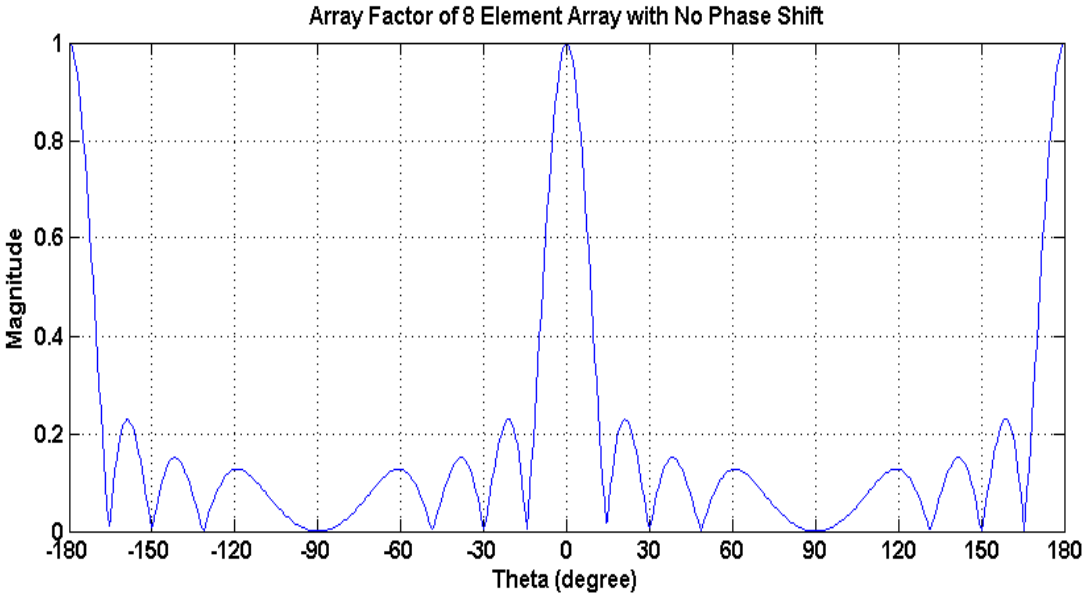

Figure 2.2: AF for 8-Element Array with $d = \frac{\lambda}{2}$, No Phase Shift

2.2. Beam Scanning

Beam scanning can be defined as the alteration of the direction of the main beam. Beam scanning in electronically scanned antennas is achieved by using two methods: phase scanning and frequency scanning.

2.2.1. Phase Scanning

Electronic scanning is fulfilled by applying a phase shift from element to element across the array. As a result of this the maximum value of the pattern points to the angle theta instead of broadside to the array axis [11].

The array factor of the array can be written as,

$$AF = a_0 \sum_{n=0}^{N-1} e^{-jn\psi_n} e^{jnkd\sin\theta} = a_0 \sum_{n=0}^{N-1} e^{jn(kd\sin\theta - \psi_n)} = a_0 \sum_{n=0}^{N-1} e^{jn\gamma} \qquad (2.10)$$

The element to element phase difference ψ can be defined in terms of angle θ_0, which is the scan angle i.e. the direction for the maximum value of the pattern,

$$\psi_n = kd\sin(\theta_0) \tag{2.11}$$

Then,

$$\gamma = kd(\sin\theta - \sin\theta_0) \tag{2.12}$$

The array factor is a maximum when γ is equal to zero ($\theta = \theta_0$). If the phase is uniform across the array, the constant phase front of the radiated field is perpendicular to the broadside direction and the beam is along the broadside direction (θ_0 must be 0°). Likewise, one should apply an incremental phase shift to all elements of the array of kd radians in order to steer the beam to the endfire direction (along the array axis), corresponding to $\theta = 90°$. Generally, it is possible to steer the main beam to a desired direction by applying a phase taper across the array [11].

Figure 2.3 shows the array factor of an 8-element array with an array spacing close to a half wavelength if a linear phase shift of 30° is applied. It is obvious that the main beam of the antenna points to the desired direction of 30° and beam steering to the desired direction is fulfilled. The directivity of the antenna output decreases with the increase of the scan angle. It is also observed that beam width increases when the scan angle increases.

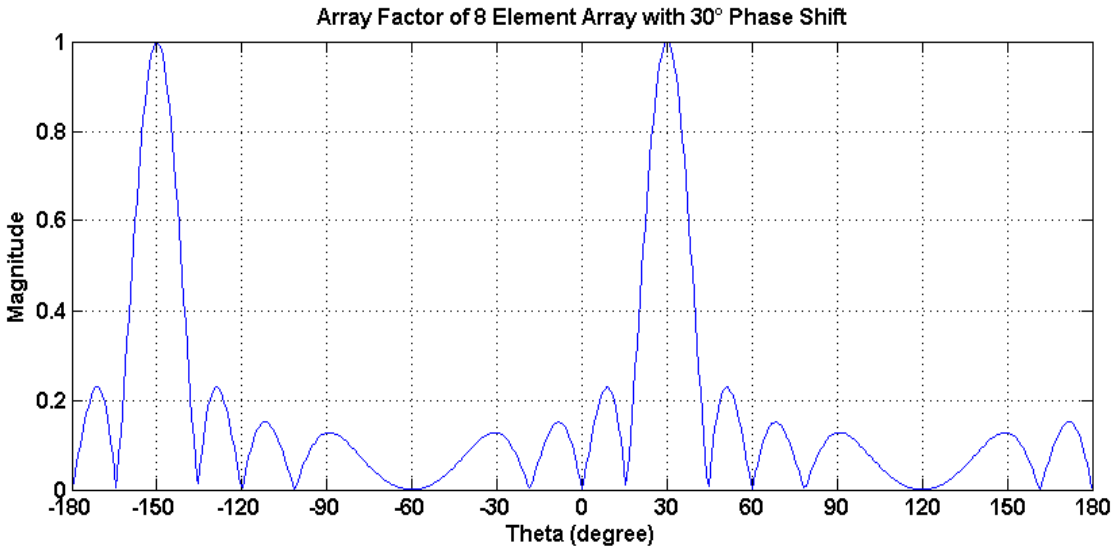

Figure 2.3: The AF for 8-Element with $d = \frac{\lambda}{2}$, 30° Phase Shift

It is possible to achieve a linear phase distribution by controlling the excitation of each radiating element separately by using electronically controlled phase shifters. Another technique which is known as frequency scanning can be used as an alternative [10]. Frequency scanning is presented in the next subsection. It provides a basis for the frequency diverse array concept.

2.2.2. Frequency Scanning

Frequency scanning is a special case of the phased array antenna where the main beam steering occurs by changing the frequency of each radiating element. Frequency scanning provides a way of beam scanning when compared to other inertialess scanning technique. This makes it more economic, reliable and relatively simple. Frequency scanning offers accurate tracking of multiple targets at widely different positions. It helps the radar provide measurements with better accuracy where the targets have high velocities and acceleration.

Air surveillance and aircraft control fields are the main areas where the widest application for frequency scanning methods has been applied. For these applications, radars have been designed and produced with antennas which are

mechanically rotated in azimuth and frequency scanned in elevation so as to provide three-dimensional aircraft position data [12].

In order to set the simple technique of frequency scanning, consider an electromagnetic wave of frequency *f*, propagating through a transmission line of length *l* and wave velocity of *v*. N·360° is the phase difference between two radiating elements at the usual frequency [11]. When the frequency changes, the angle between the axis of the main beam and the normal of the array antenna changes, too. If the transmitted frequency increases, the beam goes up the face of the antenna. If the transmitted frequency decreases, the beam goes down the face of the antenna too. The frequency scanning concept is shown in Figure 2.4.

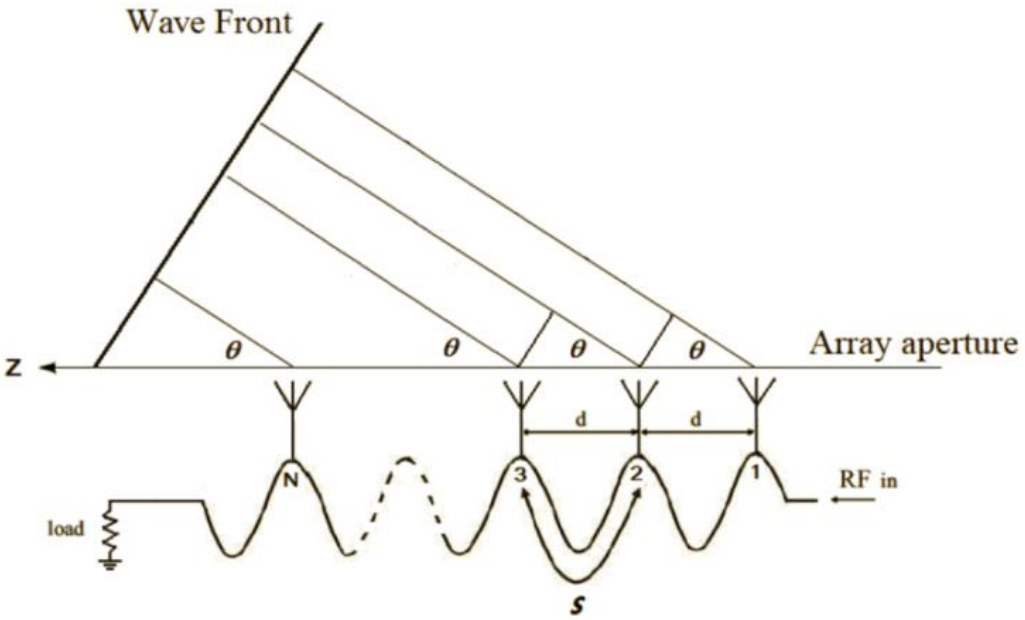

Figure 2.4: A frequency scanning array

The array factor is defined as

$$AF = a_0 \sum_{n=0}^{N-1} e^{jn\gamma} \tag{2.13}$$

where $\gamma = \frac{2\pi}{\lambda} d\cos(\theta) - \frac{2\pi}{\lambda_g} s$ and

λ is the wavelength in free space,

d is the distance between radiating elements,

λ_g is the guided wavelength in the feed line,

s is the length of feed line between elements.

The maximum value of (2.13) comes up when

$$\sin(\frac{1}{2}\gamma) = 0 \Rightarrow \frac{1}{2}\gamma \Big|_{\theta=\theta_m} = \pm m\pi \qquad m = 0,1,2... \tag{2.14}$$

Due to $s > d$, $\lambda_g > \lambda$ and $|\cos(\theta_m)| \le 1$, γ is negative. Thus,

$$\frac{2\pi}{\lambda} d\cos(\theta) - \frac{2\pi}{\lambda_g} s = -2m\pi \quad m = 0,1,2... \tag{2.15}$$

or

$$\theta_m = \cos^{-1}\left(\frac{\lambda}{d}\left(\frac{s}{\lambda_g} - m\right)\right) \qquad m = 0,1,2... \tag{2.16}$$

For a purely real maxima, the argument of the arccosine should not exceed unity. That is,

$$\left|\frac{\lambda}{d}\left(\frac{s}{\lambda_g} - m\right)\right| \le 1 \Rightarrow \frac{s}{\lambda_g} - \frac{d}{\lambda} \le m \le \frac{s}{\lambda_g} + \frac{d}{\lambda} \qquad m = 0,1,2... \tag{2.17}$$

In order not to have any grating lobes, the maximum distance between the elements should be less than $d_{\max} < \lambda/2$, because when $d < \lambda/2$ there is no more than one integer in $\left[\frac{s}{\lambda_g} - \frac{d}{\lambda}, \frac{s}{\lambda_g} + \frac{d}{\lambda}\right]$.

The inter-element path lengths are not equal in frequency scanned arrays. The increasing line lengths along the array introduces a linearly progressive phase shift, and the frequency-sensitive properties of the transmission line result in a scan with changing frequency [3].

For example, the array factor of an 8-element frequency scanning array with $d = 0.5m$, $s = 1m$ and $\sqrt{\varepsilon_{re}} = 1$ is computed using (2.13) when f is 280 MHz, 300MHz and 320MHz shown in Figure 2.5 to Figure 2.7, respectively. One can see that the main beam scans from 188° to 172° with the frequency increasing from 280MHz to 320MHz.

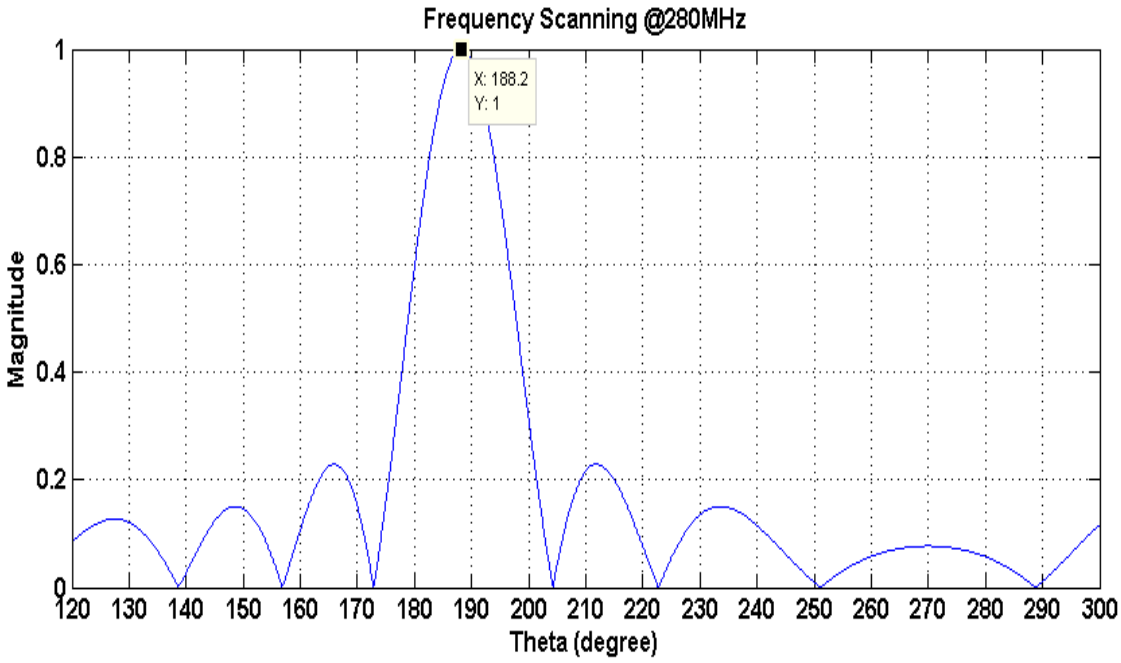

Figure 2.5: The AF of frequency scanning array at 280 MHz

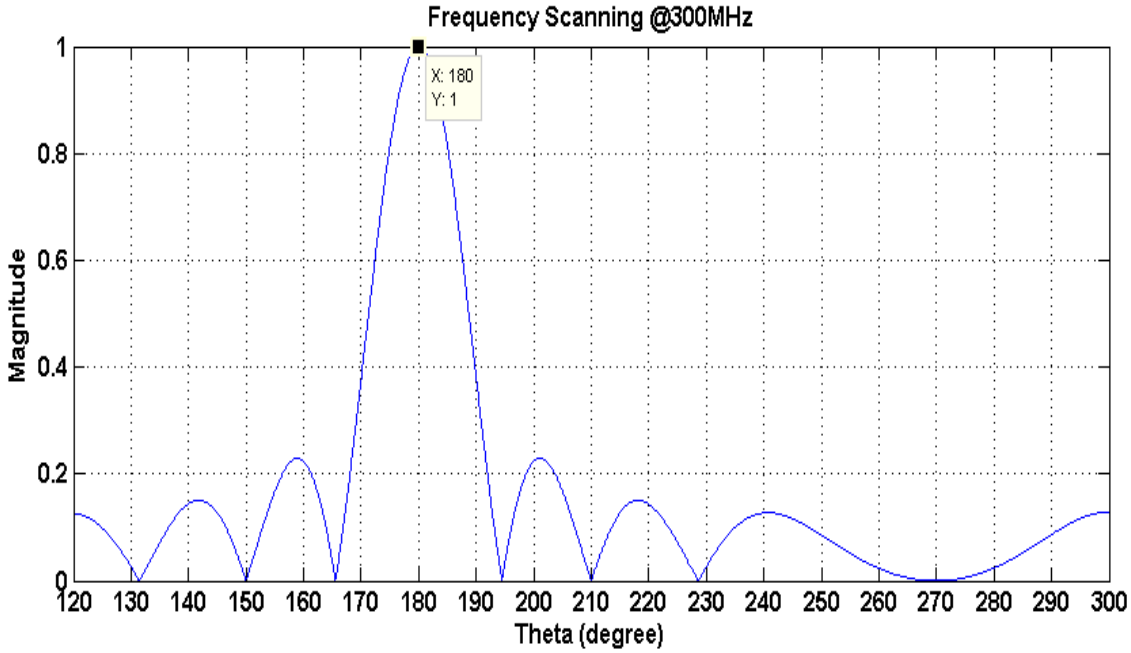

Figure 2.6: The AF of frequency scanning arrays at 300 MHz

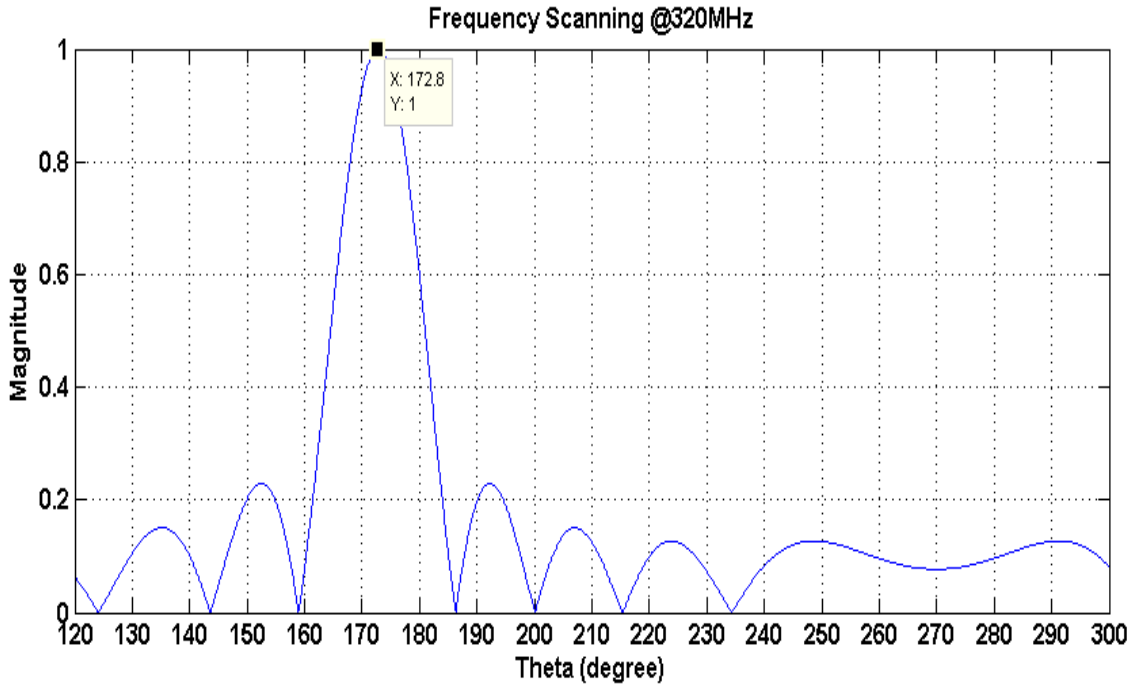

Figure 2.7:The AF of frequency scanning array at 320 MHz

This chapter discussed conventional array theory, including phased and frequency scanned arrays. A key characteristic of the frequency scanned array is that the same signal is applied to all radiating elements, and frequency is varied over time to change the beam steering angle. The next chapter will discuss the conceptual development of a frequency diverse array. It is fundamentally different than the frequency scanned array in that it applies different signals of various frequencies simultaneously to each spatial channel. It will be shown that this provides additional degrees of freedom for the control of antenna patterns [13].

CHAPTER 3

FREQUENCY DIVERSE ARRAY (FDA) CONCEPT

3.1. Background

The antenna elements of the array are excited by sources of discrete frequencies, where the frequency of each subsequent antenna is offset by a small amount of frequency in Frequency Diverse Array (FDA) concept [18]. The elements of the array can be either fed by the same waveform or different types of waveforms. The same waveform use will be assumed for simplicity in this thesis study. The most significant difference between a frequency diverse array and a conventional array is that instead of using a linear phase shift, a small amount of frequency increment compared to the carrier frequency is utilized across the array elements [11]. The progressive frequency change among the antenna elements results in continuous steering in space [15]. A far field electric pattern which is a function of range, time and angle is generated by utilization of the frequency increment. Range-dependent beam-forming is vital since local maxima can be obtained at different ranges, which can be used for multiple target detection by the help of advanced signal processing techniques. The range ambiguities may cause a problem, though [11].

3.2.Theory

Conventional array theory was dealt with in detail in Chapter 2. The use of frequency increment across the array elements is the main difference between a frequency diverse array and a conventional array. The waveform radiated by the array elements is assumed to be identical in conventional arrays, except from the amplitudes and phases. It should be taken into consideration that the side-lobe levels are reduced by amplitude tapering and progressive phase increment changes the direction of the main beam in a desired way [11].

The frequency diverse array gives additional flexibility when designing array antennas. The baseline configuration of a frequency diverse array is that a continuous wave signal is radiated from each spatial channel. A small frequency shift, on the order of a few Hertz, is applied between channels. This small frequency shift results in a beam pattern for which the beam focus direction changes as a function of range, angle and time. This is significantly different than the conventional phased array, where the beam pointing direction is independent of range and time in the far-field [13].

FDA analysis together with the extraction of the critical design parameters will be presented together in this chapter. The far field array pattern of FDA will be established in time domain. The concept of a frequency diverse array is shown in Figure 3.1. Suppose that the waveform radiated from each antenna element is the same with a frequency increment of Δf Hz applied across the elements.

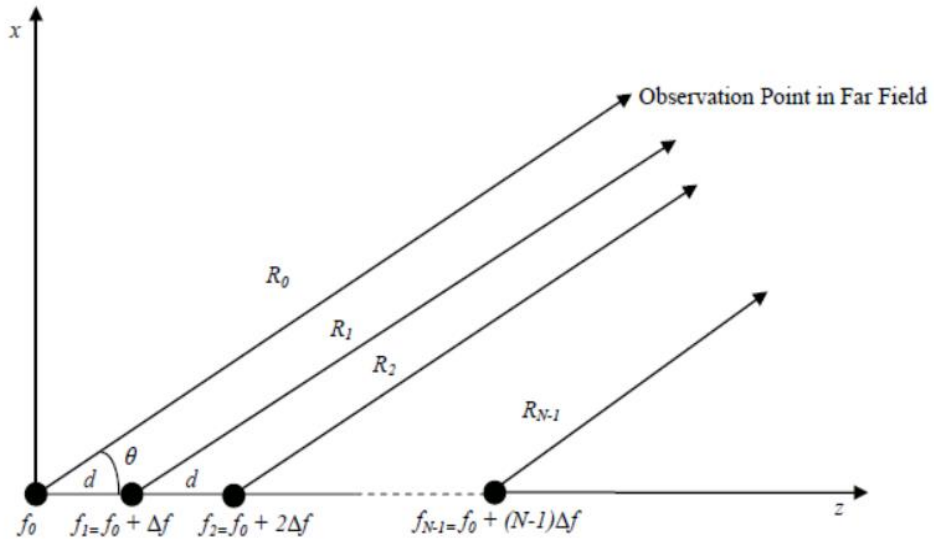

Figure 3.1: Frequency Diverse Array Antenna Concept

The phase of the excitation signal at element N, which is located in the z-axis in Figure 3.1, is

$$\psi_n = (k_0 + n\Delta k)R_n \tag{3.1}$$

In (3.1);

$$R_n = R_0 - nd\cos(\theta) \tag{3.2}$$

$$k(n) = k_0 + n\Delta k \tag{3.3}$$

$$k_0 = \frac{\omega_0}{c}$$
$$\Delta k = \frac{\Delta\omega}{c} \tag{3.4}$$

where ω_0 is the angular frequency of the waveform which is radiated from element N, R_n is called the path length between the element and the far-field observation point, θ is the angle position of the observation point in azimuth and d is the inter-element spacing.

Expanding all terms in (3.1)

$$\psi_n = \left(k_0 + n\Delta k\right)\left(R_0 - nd\cos(\theta)\right) \tag{3.5}$$

Distinguishing the elements depending on the antenna indices in (3.5),

$$\psi_n = k_0 R_0 + k_0 nd\cos(\theta) - n\Delta k R_0 + n^2 \Delta kd\cos(\theta) \tag{3.6}$$

The phase difference between the signals that arrive at element zero and element one is

$$\Delta\psi = \underbrace{k_0 d\cos(\theta)}_{First-term} - \underbrace{\Delta k R_0 + \Delta kd\cos(\theta)}_{Second-term} \tag{3.7}$$

The first term in (3.7) is nothing but the conventional array factor which appears frequently in array theory. The second term is significant as it illustrates that the range and the frequency increment altogether determine the radiation pattern of the array. Frequency scanning and frequency diverse arrays are similar in terms of frequency diversity, but the frequency increment is used as a function of time for all elements by frequency scanned arrays whereas frequency diverse arrays utilize the frequency increment at the discrete points of the aperture [13].

The new terms shown in (3.7) produce an apparent angle which is contradictory to the scan angle one normally sees. It is possible to acquire this apparent scan angle by using the same approach introduced in Chapter 2. As there is a change in the angle, progressive phase shift has to be defined in terms of the apparent angle as follows:

$$\Delta\psi = kd\cos(\theta_a) \tag{3.8}$$

where θ_a is the apparent angle. Equating (3.8) to (3.7) results in

$$\Delta\psi = kd\cos(\theta_a) = k_0 d\cos(\theta) - \Delta k R_0 + \Delta kd\cos(\theta) \tag{3.9}$$

Solving (3.9) for the angle yields the following [14]:

$$\cos(\theta_a) = \frac{f_0 \cos(\theta)}{f} - \frac{\Delta f R_0}{fd} + \frac{\Delta f \cos(\theta)}{f} \tag{3.10}$$

$$\theta_a = \arccos\left(\frac{f_0 \cos(\theta)}{f} - \frac{\Delta f R_0}{fd} + \frac{\Delta f \cos(\theta)}{f}\right) \tag{3.11}$$

According to the antenna array theory which was discussed in Chapter 2, a progressive phase shift of $\Delta\psi$ across the elements has to be used for beam scanning. Furthermore, a scan angle θ_0 has to be defined to steer the main beam to the desired direction. The amount of phase shift for an FDA is defined by (3.9), and it is possible to calculate the array factor by using a similar approach. Suppose that it is expected to steer the main beam to broadside where θ_0=90°, which means that there isn't a phase shift owing to the path length and the first term in (3.9) disappears. Moreover, suppose that uniform excitation is used and the frequency increment across the antenna array element is not applied ($\Delta f=0$). It is obvious that when θ_0=0° and $\Delta f=0$, the inter-element phase shift becomes zero ($\Delta\psi$). This is a uniform linear array configuration [11].

As an example a "range-angle dependent beam pattern" is shown Figure 3.2. where the element spacing is λ/2 and frequency increment is 15 kHz

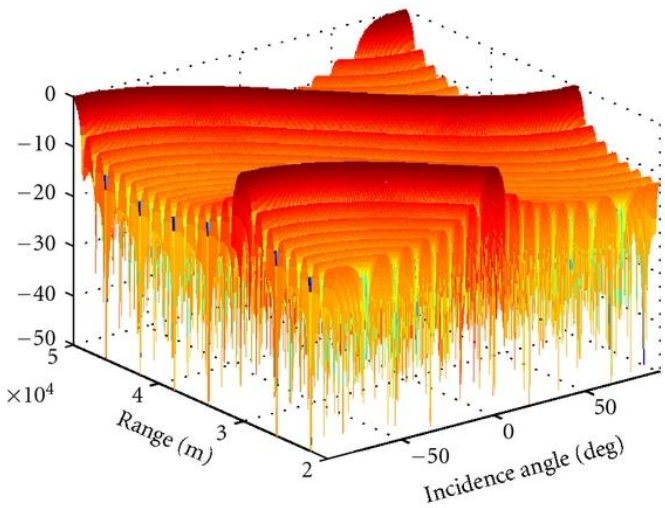

Figure 3.2: Range-Angle dependent beam pattern

When the frequency increment Δf is non-zero for the same array configuration, the second and third terms become non-zero and these terms affect the array pattern. It shows that the array pattern is both a function of time, angle and range. Therefore, the array pattern attaints to its maximum at different ranges and angles. This feature is unusual since different types of new radar operations may be supported by it. This feature can be applied to electronic warfare where a fast-moving target might egress from air defense along a diagonal line. The FDA pattern has a main peak which varies in both range and angle. As a result diagonal tracking might be improved [11].

Even though the array patterns shown in Figure 3.2 are the spatial patterns, in order to see the dependency in far-field (Figure 3.7), the electric fields that are radiated from the array elements have to be defined in terms of time and frequency increment Δf. In this section, only the array factor in the elevation plane is taken into consideration.

The far field array pattern can be rewritten as follows:

$$E_A = \sum_{n=0}^{N-1} \frac{a_n}{R_n} f_e(\omega_0 + n\Delta\omega) e^{j(\omega_0 + n\Delta\omega)t} e^{-jk(n)R_n} e^{-jn\delta} \tag{3.12}$$

where δ_n is the excitation phase of the n[th] antenna, a_n is an amplitude weighting factor of the n[th] antenna element and $f_e(\omega)$ is the element pattern of the antenna in the elevation. In Equation (3.12), phase shifters are added at each antenna element. The benefits of adding the phase shifters will be explained in the following sections. If all elements are assumed to be synchronized, the $e^{-jn\delta}$ term is dropped from (3.12). (3.1) can be rewritten as

$$\psi_n = (\omega_0 + n\Delta\omega)t - (k_0 + n\Delta k)R_n - n\delta \tag{3.13}$$

Expanding all terms in (3.13)

$$\psi_n = (\omega_0 + n\Delta\omega)t - (k_0 + n\Delta k)(R_0 - nd\cos(\theta)) - n\delta \tag{3.14}$$

In Equation (3.14), distinguishing the elements depending on the antenna indices,

$$\psi_n = \omega_0 t - k_0 R_0 + n(\Delta\omega t + k_0 d\cos(\theta) - \Delta k R_0 + n\Delta k d\cos(\theta) - \delta) \tag{3.15}$$

Suppose that the interelement frequency step is a lot smaller than the start frequency of the array, or

$$(N-1)\Delta\omega << \omega_0 \tag{3.16}$$

So Equation (3.15) can be rewritten as

$$\psi_n = \omega_0 t - k_0 R_0 + n(\Delta\omega t + k_0 d\cos(\theta) - \Delta k R_0 - \delta) \tag{3.17}$$

$$\psi_n = \omega_0 t - k_0 R_0 + n(\varphi) \tag{3.18}$$

$$\varphi = \Delta\omega t + k_0 d\sin(\theta) - \Delta k R_0 - \delta \tag{3.19}$$

Substituting these equations in (3.12) yields

$$E_A = \sum_{n=0}^{N-1} \frac{a_n}{R_n} f_e(\omega_0 + n\Delta\omega) e^{j(\omega_0 t - k_0 R_0)} e^{j(n\varphi)} \tag{3.20}$$

Assume that $f_e(\omega_0 + n\Delta\omega) \approx f_e(\omega_0)$ and $R_n \approx R_0$ in amplitude sense, (3.20) becomes

$$E_A = \frac{f_e(\omega_0) e^{j(\omega_0 t - k_0 R_0)}}{R_0} \sum_{n=0}^{N-1} a_n e^{j(n\varphi)} \tag{3.21}$$

Equation (3.21) is necessary to understand the FDA concept. In this Equation (3.21), the element pattern $f_e(\omega_0)$ is multiplied with the array pattern that is dependent on time, angular bearing and range of the observation point and the complex weighting of each channel. Here, for the ease of mathematical expressions, unity i.e. $a_n = 1$ for all elements can be assumed for the amplitude weighting of each channel.

Equation (3.21) becomes

$$E_A = \frac{f_e(\omega_0) e^{j(\omega_0 t - k_0 R_0)}}{R_0} \sum_{n=0}^{N-1} e^{j(n\varphi)} \tag{3.22}$$

In (3.22), the summation term can be rewritten as [2]

$$\sum_{n=0}^{N-1} e^{j(n\varphi)} = e^{j\left(\frac{N-1}{2}\right)\varphi} \frac{\sin\left(N\frac{\varphi}{2}\right)}{\sin\left(\frac{\varphi}{2}\right)} \tag{3.23}$$

Using Equation (3.23) in (3.22),

$$E_A = \frac{f_e(\omega_0) e^{j(\omega_0 t - k_0 R_0)}}{R_0} e^{j\left(\frac{N-1}{2}\right)\varphi} \frac{\sin\left(N\frac{\varphi}{2}\right)}{\sin\left(\frac{\varphi}{2}\right)} \tag{3.24}$$

And the real part of the elevation electric field becomes (ignoring the element pattern since the array pattern is the subject of this thesis)

$$\mathrm{Re}\{E_A\} = \frac{\cos(\omega_0 t - k_0 R_0 + \frac{N-1}{2}\varphi)}{R_0} \frac{\sin\left(N\frac{\varphi}{2}\right)}{\sin\left(\frac{\varphi}{2}\right)} \tag{3.25}$$

Since φ has time dependent terms, we can expand (3.25) using (3.19).

$$\mathrm{Re}\{E_A\} = \frac{1}{R_0}\cos(\omega_0 t - k_0 R_0 + \frac{N-1}{2}\Delta\omega t + \frac{N-1}{2}k_0 d\cos(\theta) - \frac{N-1}{2}\Delta k R_0 - \frac{N-1}{2}\delta) \frac{\sin\left(N\frac{\varphi}{2}\right)}{\sin\left(\frac{\varphi}{2}\right)} \tag{3.26}$$

Grouping the terms in (3.26)

$$\mathrm{Re}\{E_A\} = \frac{1}{R_0}\cos((\omega_0 + \frac{N-1}{2}\Delta\omega)t - (k_0 + \frac{N-1}{2}\Delta k)R_0 \underbrace{+\frac{N-1}{2}(k_0 d\cos(\theta) - \delta)) \frac{\sin\left(N\frac{\varphi}{2}\right)}{\sin\left(\frac{\varphi}{2}\right)}}_{Last-part} \tag{3.27}$$

Equation (3.27) shows that the amplitude modulation of a continuous wave signal at frequency $\omega_0 + \frac{N-1}{2}\Delta\omega$ has dependence on the last part in (3.27), i.e. time, range and observation angle. The term $1/R_0$ in (3.27) is called the fall-off factor of the far electric field which results from range [11].

The design equations for the array operation can be obtained from the modulation term, this is fulfilled in the next sub-section.

3.3.The Periodicity of the Radiation Array Pattern

The periodic radiation array pattern in angle, time and range is shown by using MATLAB. First of all, the periodicity of the pattern in time will be illustrated when the range and angle θ are fixed. In simulations, parameters used are tabulated in Table 3.1. Suppose that the position of the first element of the array is selected as origin, which will cause extra phase terms in the far field radiation pattern.

Table 3.1: Simulation Parameters

Parameter	Value
Start Frequency	320MHz
Frequency Step	10kHz
Number of Array Elements	8
Range	30km
Broadside of the array	90°

According to Equation (3.28), φ is a function of range, angle and time. Therefore, many solutions exist for this equation. Furthermore, the phase term offers flexibility in (3.28), φ can be controlled by changing the phase of each antenna element.

$$\varphi = \Delta\omega t + k_0 d\cos(\theta) - \Delta k R_0 - \delta = 2m\pi \tag{3.28}$$

The periodicity in time can be computed with (3.28) for the following values of m.

$$\Delta\omega t_0 + k_0 d\cos(\theta) - \Delta k R_0 - \delta = 2\pi * 0$$

$$\Delta\omega t_1 + k_0 d\cos(\theta) - \Delta k R_0 - \delta = 2\pi * 1$$

$$\Delta t = t_1 - t_0 = \frac{1}{\Delta f} = \frac{1}{10kHz} = 100us \tag{3.29}$$

The modulating waveform which has the properties given in Table 3.1 is shown in Figure 3.3. It is obvious that the time difference between the two peaks is 100us. The period of the time-dependent array pattern matches the calculated one using the derived equation.

The null-to-null beamwidth is a significant parameter of radar applications. Using $\frac{N\varphi}{2} = m\pi$, the null-to-null beamwidth can be calculated as

$$\Delta t_{null-to-null} = \frac{4\pi}{N\Delta\omega} = \frac{2}{N\Delta f} = \frac{2}{8x10kHz} = 25us \tag{3.30}$$

which is seen in Figure 3.3.

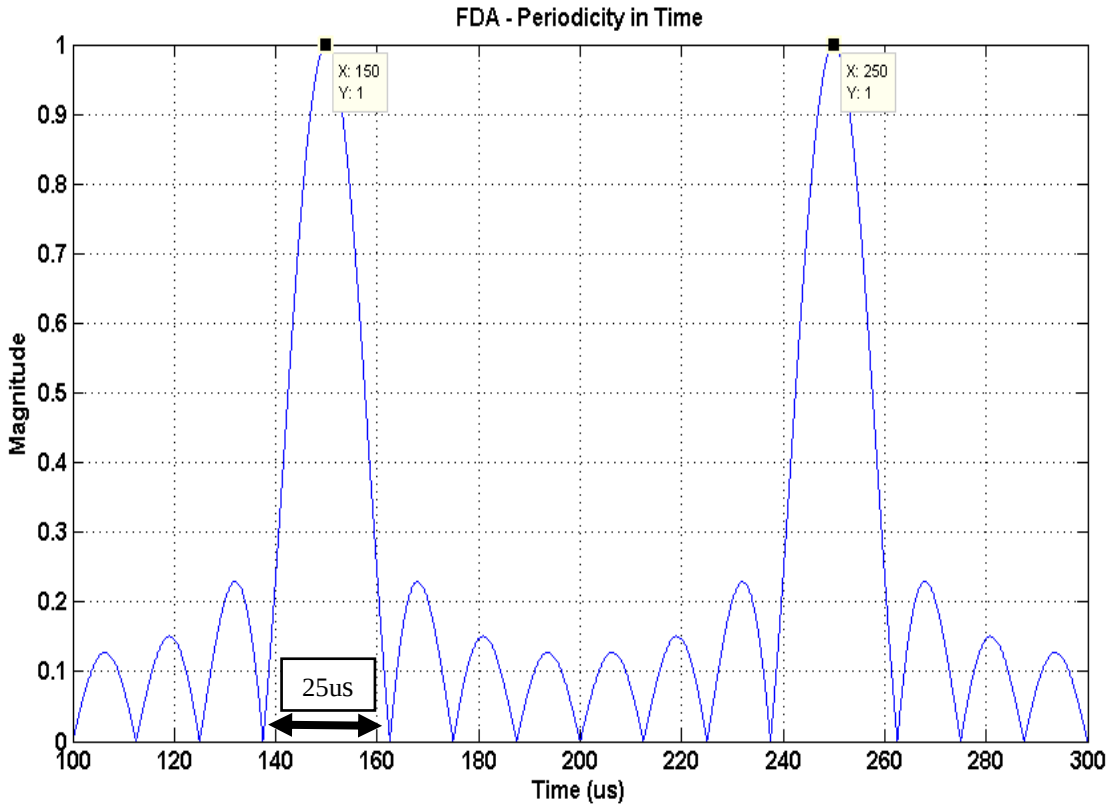

Figure 3.3 Time-dependent Array Pattern (Periodicity in Time)

Similarly, if phase and time are fixed, range periodicity can be computed with (3.30):

$$\Delta\omega t + k_0 d\cos(\theta) - \Delta k R_0 - \delta = 2\pi * 0$$

$$\Delta\omega t + k_0 d\cos(\theta) - \Delta k R_1 - \delta = 2\pi * 1$$

$$\Delta R = R_1 - R_0 = \frac{c}{\Delta f} = \frac{3x10^8 m/s}{10kHz} = 30km \tag{3.31}$$

The range-dependent array pattern is simulated for a fixed time (*t=100us)* and angle ($\theta = 90°$) by using the parameters in Table 3.1. It can be clearly seen that the periodicity of range dependent pattern is 30 km in Figure 3.4, which is consistent with the period calculated in (3.30).

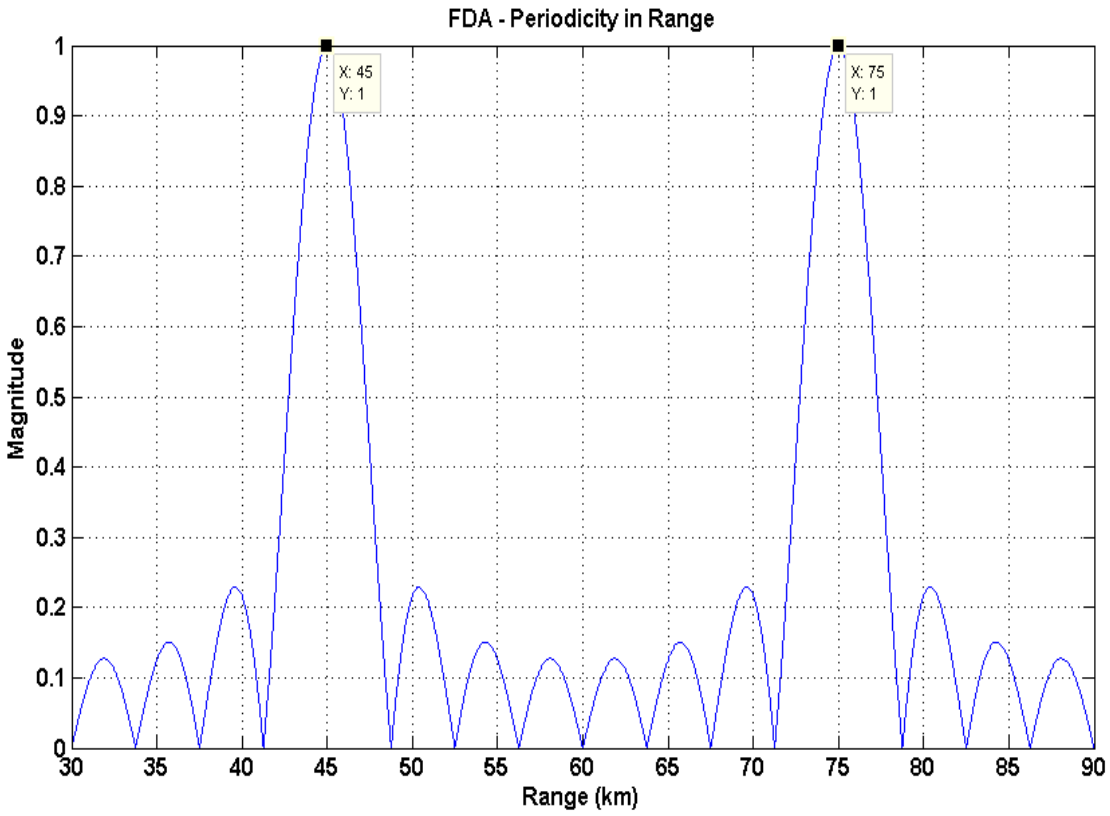

Figure 3.4 Range-dependent Array Pattern (Periodicity in Range)

The periodicity in $\cos(\theta)$ can be found as

$$\Delta\cos(\theta) = \frac{2\pi}{k_0 d} = \frac{\lambda}{d} = \frac{\lambda}{\lambda/2} = 2 radians \tag{3.32}$$

Finally, the angle-dependent array pattern is plotted in MATLAB for a fixed value of time (*t=100us*) and range (R_0 *=30km*). The resulting graph is given in Figure 3.5

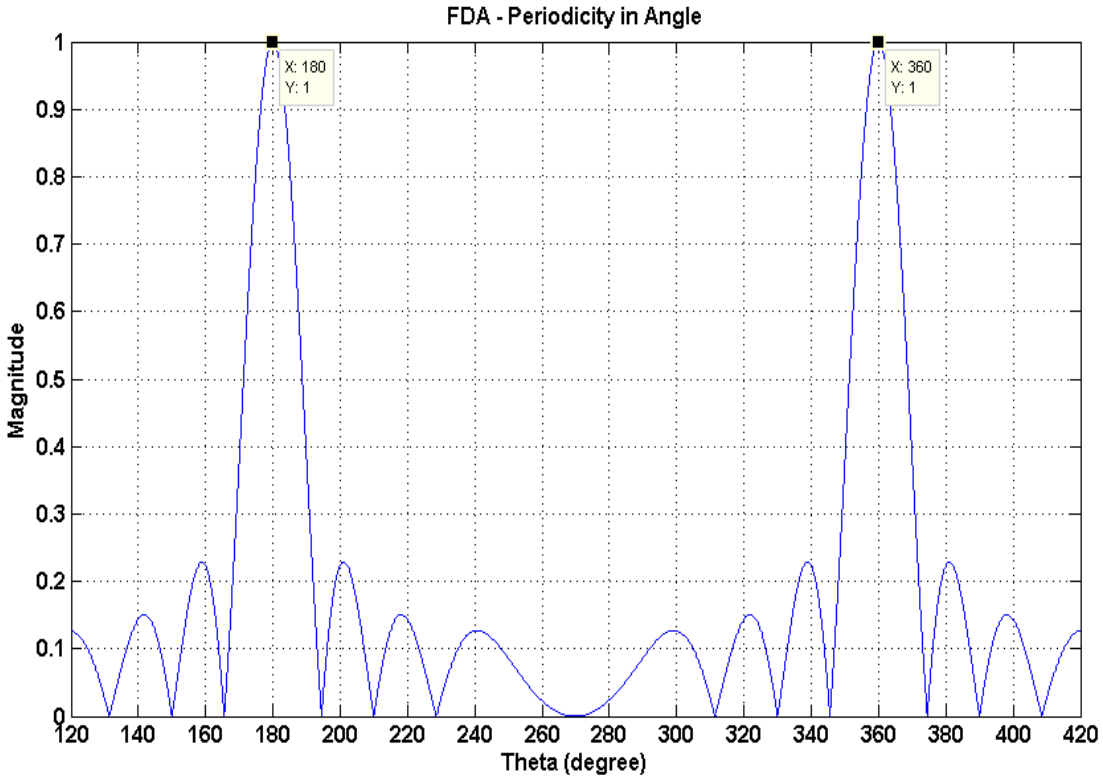

Figure 3.5 Angle-dependent Array Pattern (Periodicity in Angle)

Based on Figure 3.5, the period of the angle-dependent pattern is 180 degrees. It was found to be $\frac{\lambda}{d}$ radians by using (3.31), which is the same value when $d = \frac{\lambda}{2}$.

To conclude this subsection, the periodicity of the pattern in angle, range and time has been illustrated in Figures 3.3, 3.4, and 3.5.

3.4.Understanding How FDA Mechanism Works

The FDA mechanism built upon the fact that each antenna element's frequency is different from others. Therefore, time and range dependencies are based on the frequency difference between sequential antenna elements in the array. Furthermore, suppose that all frequency components over the aperture of the array are in-phase at $t = 0$ but due to different frequencies, the points where the frequency components become in-phase will depend on the position in space and the time of travel of wave components.

The points where the frequency components are in phase, in other words when (3.28) is satisfied, the beam peaks are observed in space. The interference is an easy-to-understand phenomenon with a basic example as shown in Figure 3.6, where 8 waves with frequencies tabulated in Table 3.2 are superimposed on the same graph. Note that $\Delta\omega = 2\pi 50Hz$, requiring 20 milliseconds of beam periodicity in time according to (3.29), is also visible in Figure 3.6 [2].

Table 3.2: Frequencies of simulated in Figure 3.6

Channel Number	Frequency(Hz)
1	50
2	100
3	150
4	200
5	250
6	300
7	350
8	400

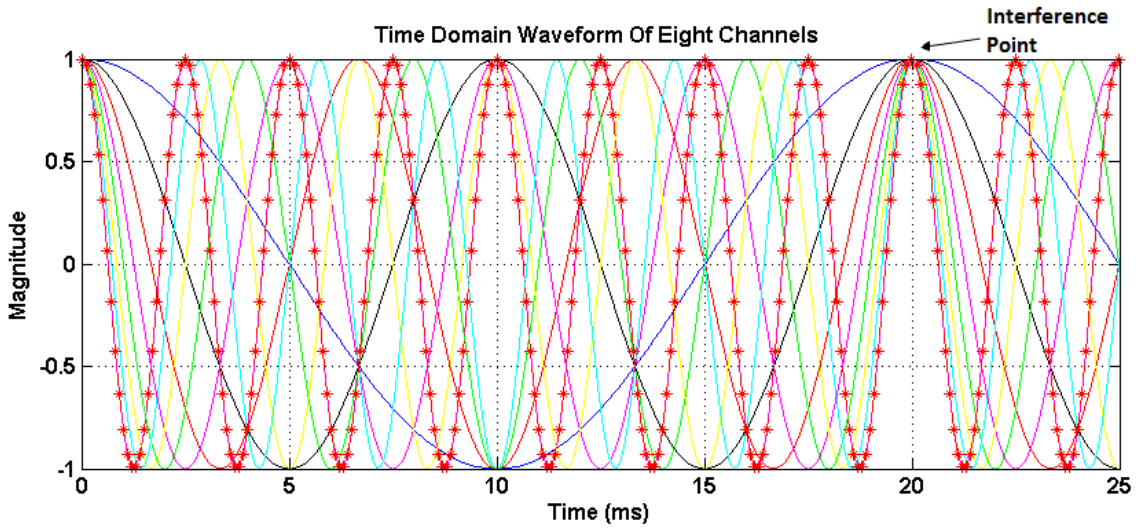

Figure 3.6: Interference of 8 Waves

Since the components travel in the space with the velocity of light, the modulation in time also leads to modulation in range. Because of this, the periodicity in range is just the product of the velocity of wave components, c, with the periodicity in time as apparent from (3.29) and (3.30).

The angle dependency results from the inter-element spacing. For different observation angles, the points of interference should shift since, for each angle of interest, the wave components propagating from each antenna element would have different delays (from (3.1), (3.2) and (3.3), $k(n)R_n$) and the time of interference will change in such a way to make up for the further delay.

An Array pattern simulation result of FDA is shown in Figure 3.7. There are beam bending and interference points in 2-D space. Simulations parameters are tabulated in Table 3.3.

Table 3.3: Parameters for 2-D FDA Simulation

Parameters	Value
Time	200us
Broadside Range	50km
Cross-sides	-35/65km
Number of Antenna Elements	8
Starting Frequency	320MHz
Frequency Step	25kHz

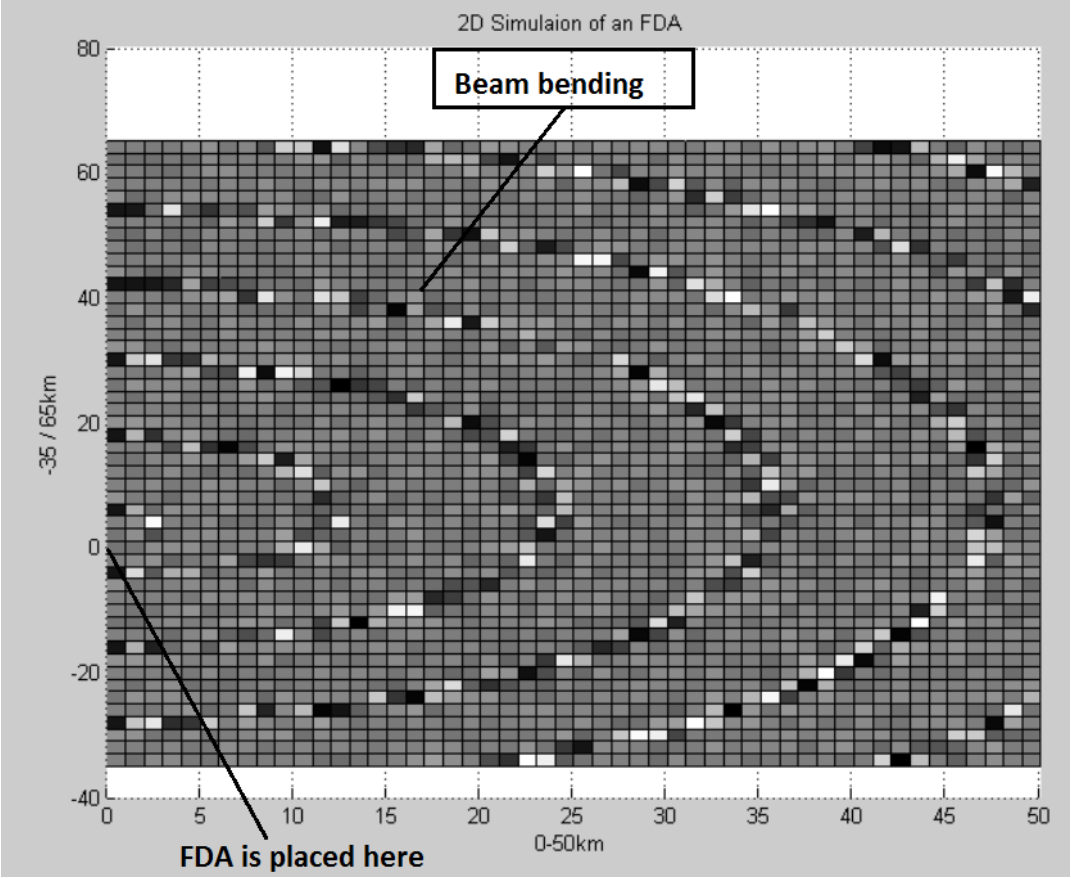

Figure 3.7: 2-D simulation of an FDA

CHAPTER 4

PHYSICAL IMPLEMENTATION OF FDA STRUCTURE

4.1. Background

When the physical implementation of FDA is concerned, there are three main frequency synthesizer types: Direct Analog Synthesizers, Indirect PLL Synthesizers, Direct Digital Synthesizers. Our research leads to the DDS (Direct Digital Synthesizer) based FDA structure because it is not convenient to achieve phase synchronization between multiple Direct Analog synthesizers. In addition the indirect PLL synthesizer has poor phase noise performance and frequency resolution. So, DDS frequency synthesizer becomes the best option. As the focus of this thesis is an examination of FDA, the details about DDS will not be gone through in this thesis. However, basic mechanisms and key parameters of DDS are discussed, as they will determine the quality of the frequency diverse signals. DDS based frequency synthesizer is not a new idea but in this thesis it is used for FDA as an effective hardware implementation approach. A bare version of DDS based FDA hardware which was mentioned in the previous chapter is implemented for the measurements. DDS based FDA beam former, oscilloscope, peak power sensor, peak power analyzer, signal generator, an I/O controller and PC would be adequate for the measurements. Three signal parameters which control the DDS are available to the user. These are frequency, phase and amplitude. Therefore, phase shifters and attenuators will not be used for implementation in this thesis.

This chapter explains basic DDS based FDA structure which is implemented. In addition, the test configuration and measurements of the FDA structure are presented for the justification of mathematical derivations. Finally, the results of the measurements and simulation graphs are compared.

4.2. Design of DDS Based FDA Beamformer

In Chapter 3, when the concept of FDA is introduced and the array factor of FDA is derived, there are two assumptions made on which further discussions are based. The first assumption is that the frequency increment Δf should be far less than the working frequency f ; while the second assumption is that all signals should have 0° phase at $t = 0$. Both assumptions are to be complied with when physically implementing the FDA.

The DDS has a phase accumulator which provides frequency tuning resolution. Commercial frequency synthesizers manage to achieve resolution in the order of μHz by utilizing a technology called direct digital synthesis (DDS). The combination of DDS/DAC can form a digitally programmable high frequency, analog output synthesizer which is able to produce a frequency agile sinusoidal waveform at frequencies up to 1 GHz.

The remaining task is to obtain frequency diverse signals separated by Δf from each other, whose phases at $t = 0$ are all 0º. The solution to this problem is a frequency diverse signal generator composed of several synchronized DDS.

4.2.1. Understanding Direct Digital Synthesis (DDS)

Figure 4.1 illustrates the block diagram of a simple DDS frequency synthesizer. a frequency reference, a numerically controlled oscillator (NCO) and a digital-to-analog converter (DAC) are the building blocks of DDS.

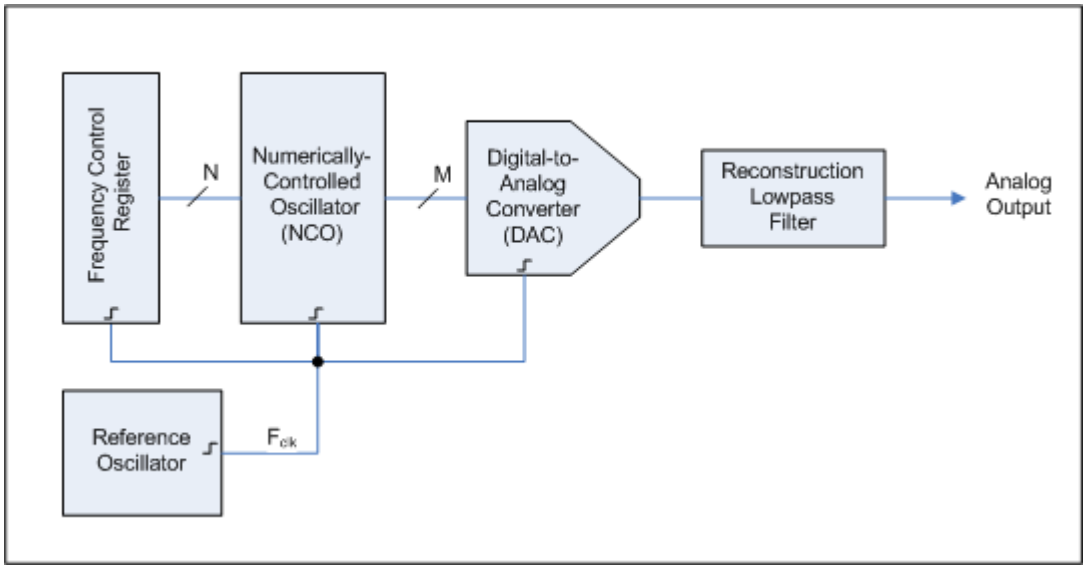

Figure 4.1 Block Diagram of the Direct Digital Synthesizer

The stable time base of the system is the reference oscillator and the frequency accuracy of the DDS is determined by the help of it. The Reference Oscillator provides the clock signal to the NCO, which generates at its output a discrete-time, quantized versions of the desired output waveform. The digital word which in the Frequency Control Register controls the period of the output signal. The DAC transforms the sampled, digital waveform into an analog waveform. The output reconstruction filter suppress the spectral replicas which are generated by the zero-order hold circuit during the analog conversion [19].

Instead of producing all samples of a waveform shown in Figure 4.2, DDS produces periodic signals at precise frequencies by choosing samples from memory. Although DDSs permit users to precisely define the waveform which is being produced, they are limited in that they are not able to achieve good frequency resolution at high frequencies.

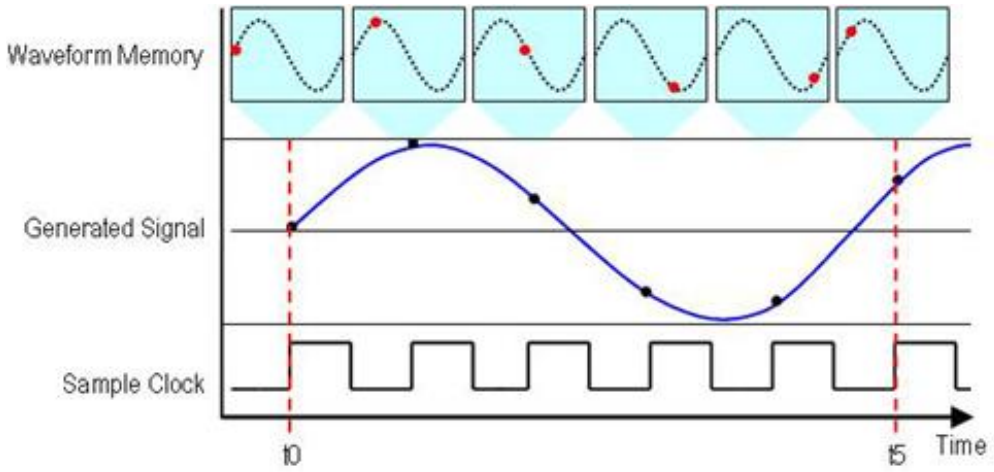

Figure 4.2 Principle Operation of DDS

4.2.1.1. Critical Parameters of a DDS

There are several important parameters of a Direct Digital Synthesizer:

Frequency range – One of the drawbacks is the range of output frequencies that can be produced by the DDS. According to the Nyquist Criteria, the clock frequency has be at least twice the output frequency. Practical limitations restrict the actual highest output frequency to about 1/3 of the clock frequency. The value which is in the frequency control register determines the output frequency of DDS.

Step size – It is the smallest frequency increment that the DDS frequency synthesizer can produce.

Phase noise – Another significant parameter is phase noise which is an indicator of the signal quality. It is the result of small random fluctuations in the phase of an signal. Also, it is a limiting factor to the dynamic range of systems. An ideal signal's total energy is concentrated in a singular frequency. Real signals have a spectral distribution, and their energy is spread. The phase noise of a synthesizer is the ratio of the carrier power to the power in a 1Hz bandwidth at a given offset frequency. It is expressed in dBc/Hz.

Spurious signals – They can be defined as harmonics in and out-of-frequency band. Spurs may come from a variety of sources. One of the most common is DDS's reference signal, which is often referred to as the reference spur. Other sources of spurious signals are generated by truncation effects of the numerically controlled oscillator (NCO).

Switching speed - The phase accumulator helps the DDS to have a faster frequency hopping and better frequency tuning resolution. Moreover, the DDS is capable of fast phase and amplitude switching.
Other critical parameters are power, supply voltage, size, interface protocol, temperature range and reliability.

4.2.2. Beam-Former with Dividers/Combiners

DDS based FDA structure is presented in this section. To complete the FDA structure, a frequency-agile source with excellent spectral purity was developed using a commercial direct-digital synthesizer (DDS). The design is based on the DDS AD9910, which is combined with a clock distribution circuitry, external LPF, combiners, and dividers.

AD9910 (DDS): has an 14-bit DAC which supports sample rates up to 1 GSPS. It uses a proprietary DDS technology which reduces power consumption without losing performance. The DDS/DAC combination forms a digitally programmable, high frequency, analog output synthesizer which generates a sinusoidal waveform at frequencies reaching 400 MHz [20].

The user can control output signal parameters of the DDS such as frequency, phase, and amplitude. The tuning resolution is 0.23 Hz with a 1 GSPS sample rate. Furthermore, the DDS is able to switch phase and amplitude on the order of μHz.

Other features of (Analog Devices) AD9910 are given below

- ✓ It has −125 dBc/Hz Phase Noise (400MHz carrier signal @ 1kHz Offset)
- ✓ It has better than 80 dB narrow-band SFDR.
- ✓ It supports serial input/output (I/O) control
- ✓ It is capable of sweeping frequency, phase, and amplitude.
- ✓ It has 8 frequency and phase offset profiles
- ✓ Its' power supplies are 1.8 V and 3.3 V
- ✓ Power down can be controlled by software and hardware
- ✓ Its package is 100-lead TQFP_EP
- ✓ It has an inverse sinc filter Sin(x)/(x) correction
- ✓ It is capable of phase and amplitude modulating
- ✓ 1024 word × 32-bit RAM is integrated in the chip
- ✓ It has a PLL REFCLK multiplier
- ✓ It supports multichip synchronization.
- ✓ It has parallel data-path interface
- ✓ Internal oscillator can be driven by a single crystal

ADCLK854 (Clock Fanout Buffer): gets a clock input from one of two inputs and sends the selected clock to all output channels. The outputs can be set to either LVDS or CMOS levels.

LFCN-320 (Low Pass Filter): DC(1) to 320 MHz, 0.78dB insertion loss

SCA-4-20 (Power Splitter): 1000 to 2000 MHz 4 way 0º

AD4PS-1 (Power Combiner): 0 to 500 MHz 4 way 0º

ADP-2-10 (Power Combiner): 5 to 1200 MHz 2 way 0º

The block diagram of the DDS based FDA beam-former network is shown in Figure 4.3. It consists of 8 DDS, clock distribution IC, reference source (1GHz) and SPI communication interface adapter (I/O Controller) for programming.

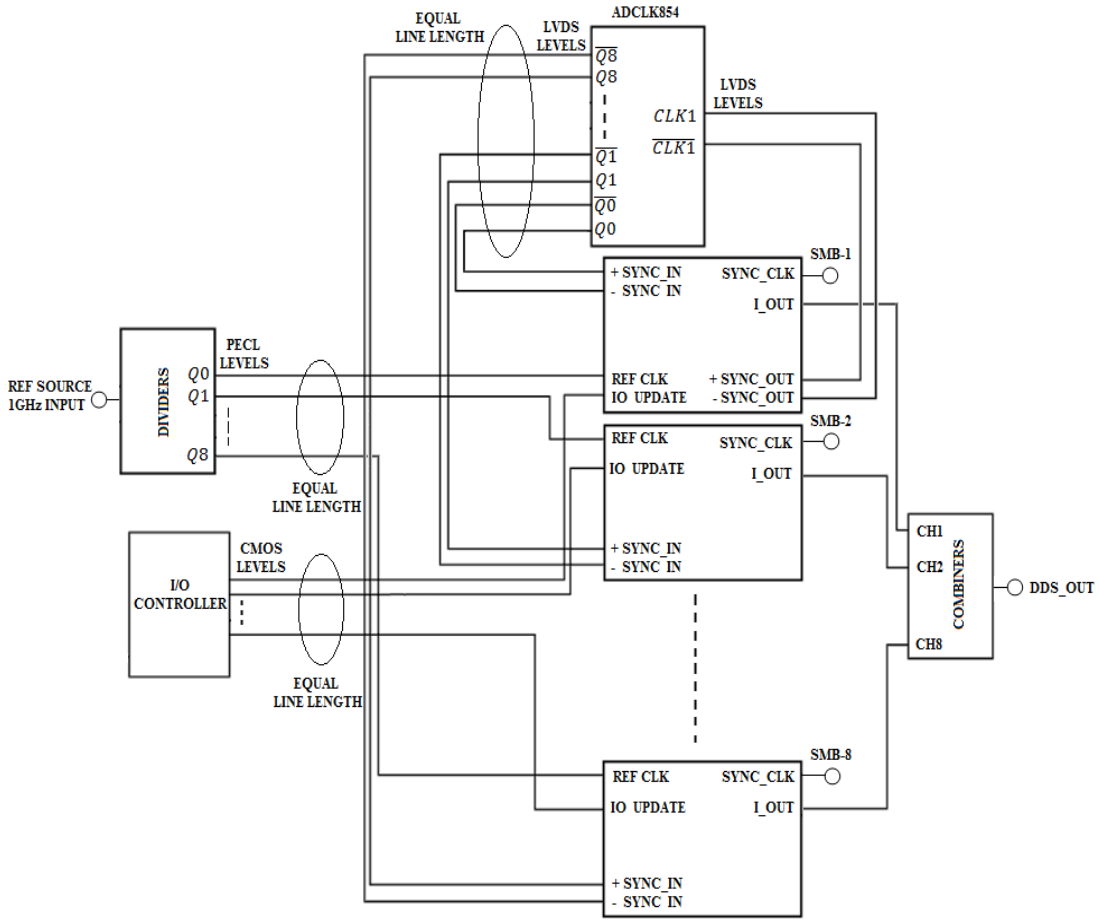

Figure 4.3 DDS Based FDA Beam-former Block Diagram

Synchronization of multiple DDS devices allows precise digital tuning of the phase and amplitude across multiple frequency carriers. The circuit in Figure 4.3 demonstrates how to synchronize eight AD9910 1 GSPS, DDS chips using the ADCLK854 clock fan-out buffer. The result is the precise phase alignment between the clock and output signals of eight AD9910 chips [21].

There are three basic requirements to synchronize multiple AD9910's:

a) The first requirement is to provide a coincident reference clock (REF CLK). To accomplish this, connections were made with matched line lengths.
b) The next step for synchronization is to align the rising edge of SYNC_CLK for all AD9910's. The SYNC_CLK provides the reference for a coincident IO_UPDATE. SYNC_CLK alignment is accomplished using the internal synchronization capability of the AD9910. The ADCLK854 distributes phase aligned SYNC_IN signals to all AD9910s.
c) The last requirement to synchronize multiple DDS devices is a coincident IO_UPDATE. This is done by having equal length line for the IO_UPDATE signals across all AD9910's. The MASTER DDS also provides a CMOS output clock to the I/O Controller for the IO_UPDATE.

See the AD9910 data sheet for more details on synchronization capability.

A photograph of the DDS based FDA beam-former is demonstrated in Figure 4.4. There are SMA connectors for the input, outputs and SYNC_CLK ports. The beam former components are tabulated in Table 4.1. For highest performance, separate regulators are used for each DDS power supply voltages which are 1.8V and 3.3V. As shown in Figure 4.5, equal line lengths are used for each DDS's input and output signal lines. Detailed schematics are shown in Figure 4.5, 4.6, 4.7 and Figure 4.8.

Table 4.1: Components used in DDS based FDA Beam Former Board

Component	Company Name/Model	Number of Pieces
DDS	Analog Devices/AD9910	8
2-Way Divider	Mini Circuits/ SCN-2-11	1
2-Way Combiner	Mini Circuits/ ADP-2-10	1
4-Way Divider	Mini Circuits/SCA-4-20	2
4-Way Combiner	Mini Circuits/ AD4PS-1	2
LPF	Mini Circuits/LFCN-320	8
Clock Dsitribution	Analog Devices/ ADCLK854	1
3.3V Regulator	MICREL/ 998-MIC37100-3.3WS	16
1.8V Regulator	MICREL/ MIC37100-1.8WS	17
5V Regulator	MICREL/MIC29502BU	2

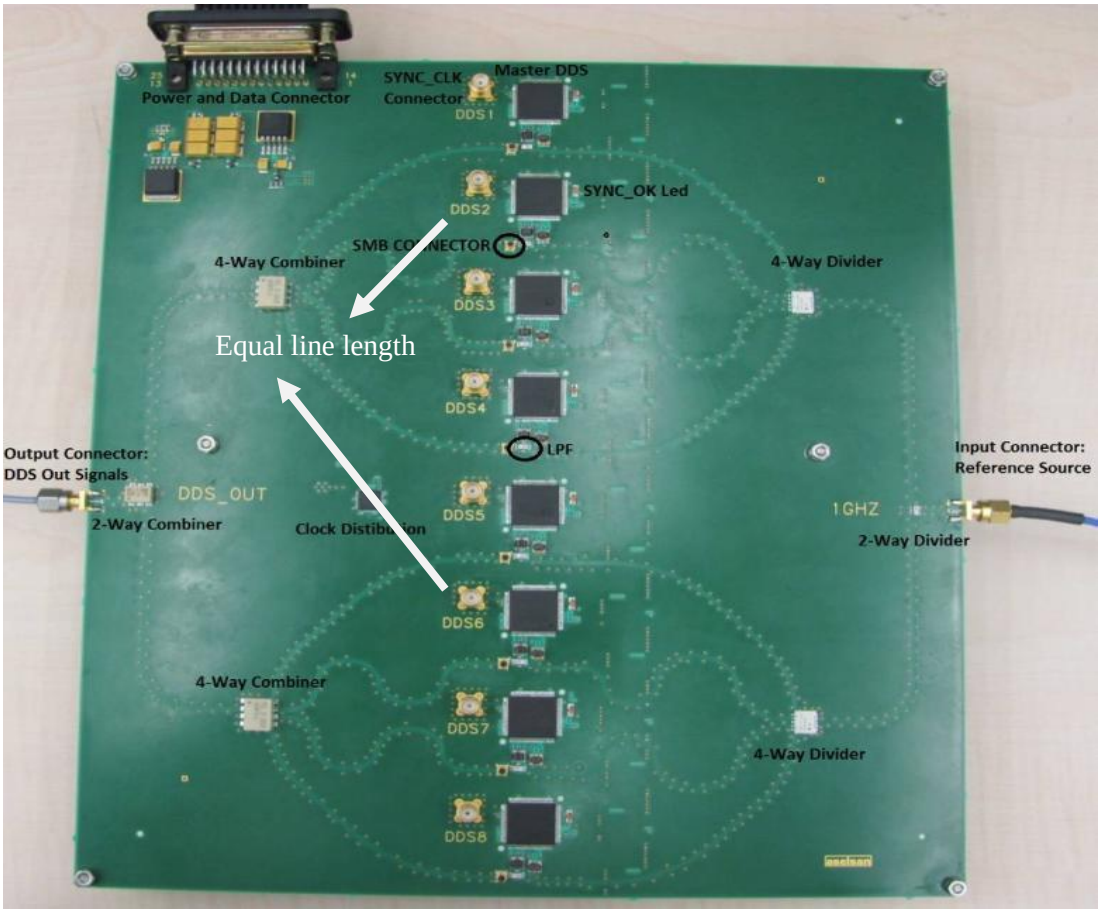

Figure 4.4 Basic DDS Based FDA Structure

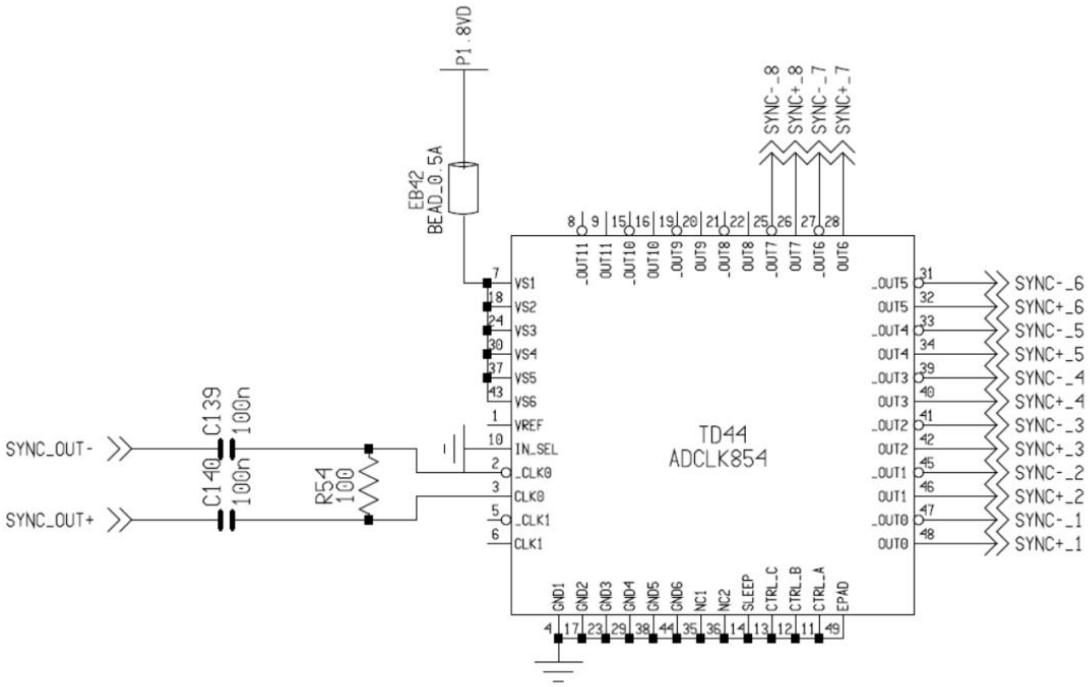

Figure 4.5 Schematic of Clock Distribution Part

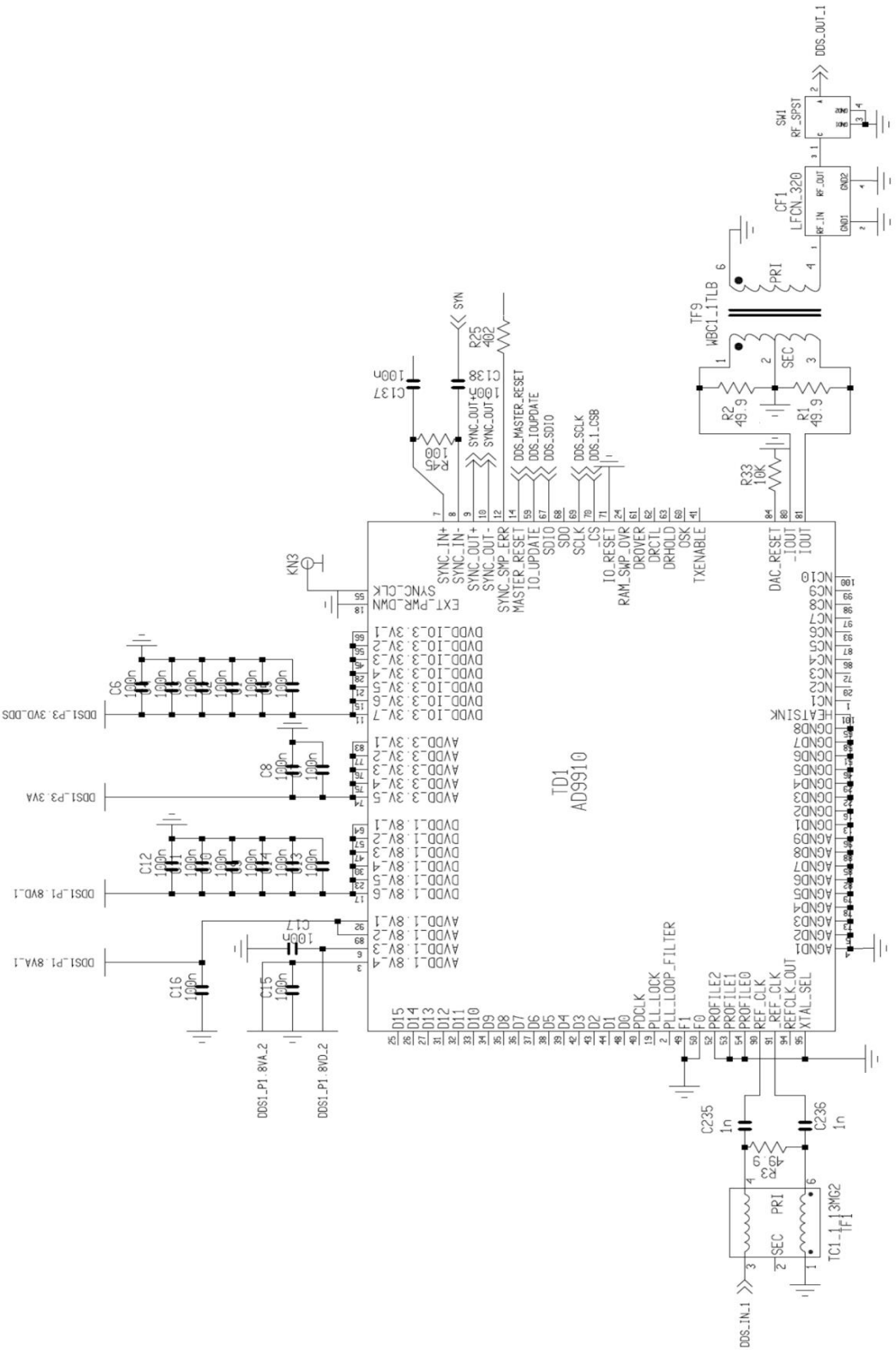

Figure 4.6 Schematic of Master DDS Part

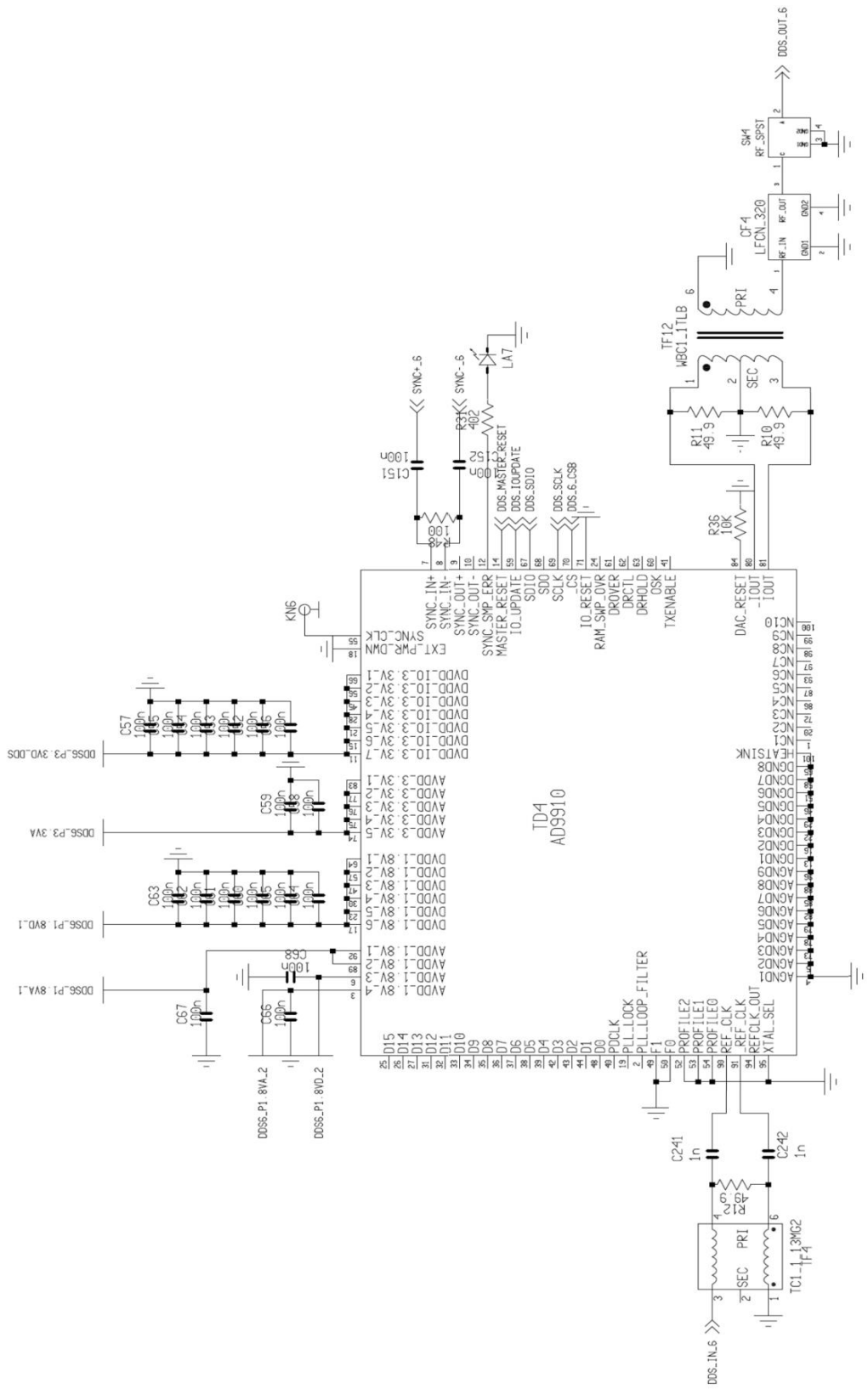

Figure 4.7 Schematic of Slave DDS Part

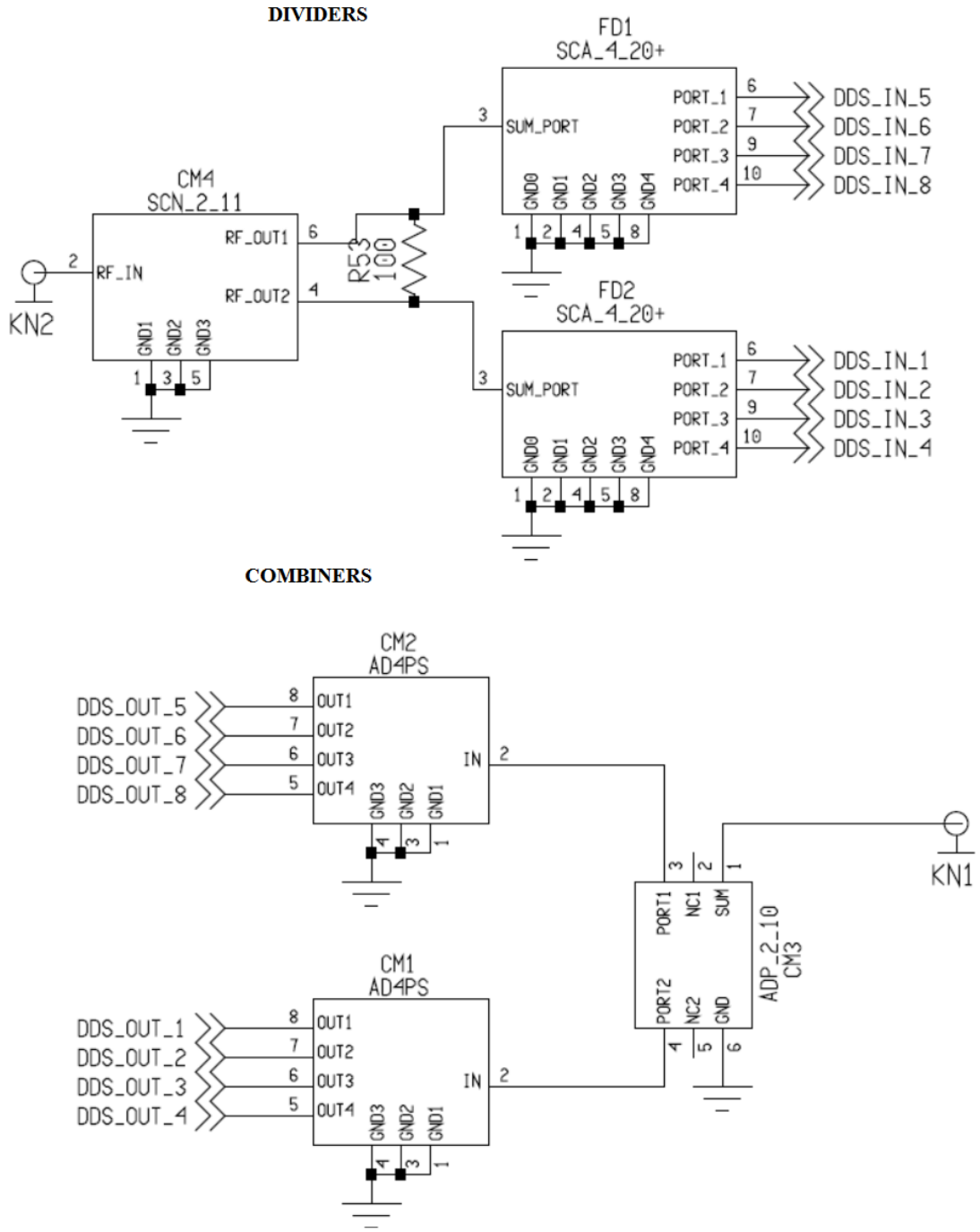

Figure 4.8 Schematic of Divider/Combiner Part

4.2.3. I/O Controller

The DDS can be programmed using an SPI interface. I/O Controller offers a Serial Peripheral Interface (SPI) adapter that one can use to connect his/her hardware to the computer. As shown Figure 4.9, I/O Controller is one of the smallest and cheapest adapter available on the market.

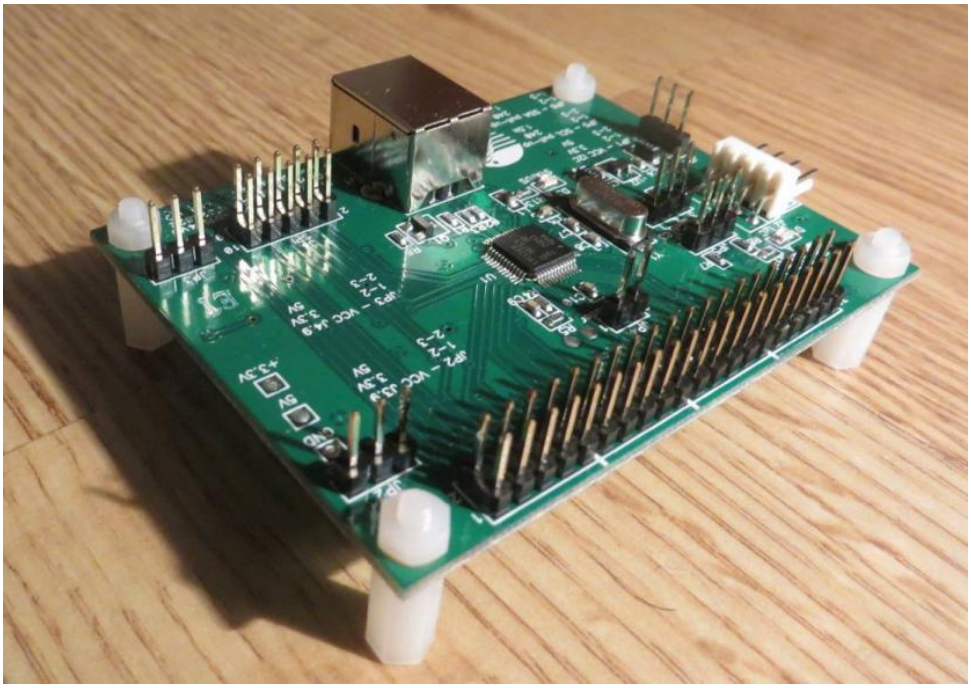

Figure 4.9 SPI Interface Adapter (I/O Controller)

4.3. User Interface For FDA Developers

A user interface as shown in Figure 4.10 was designed to configure the output frequency, phase and amplitude.

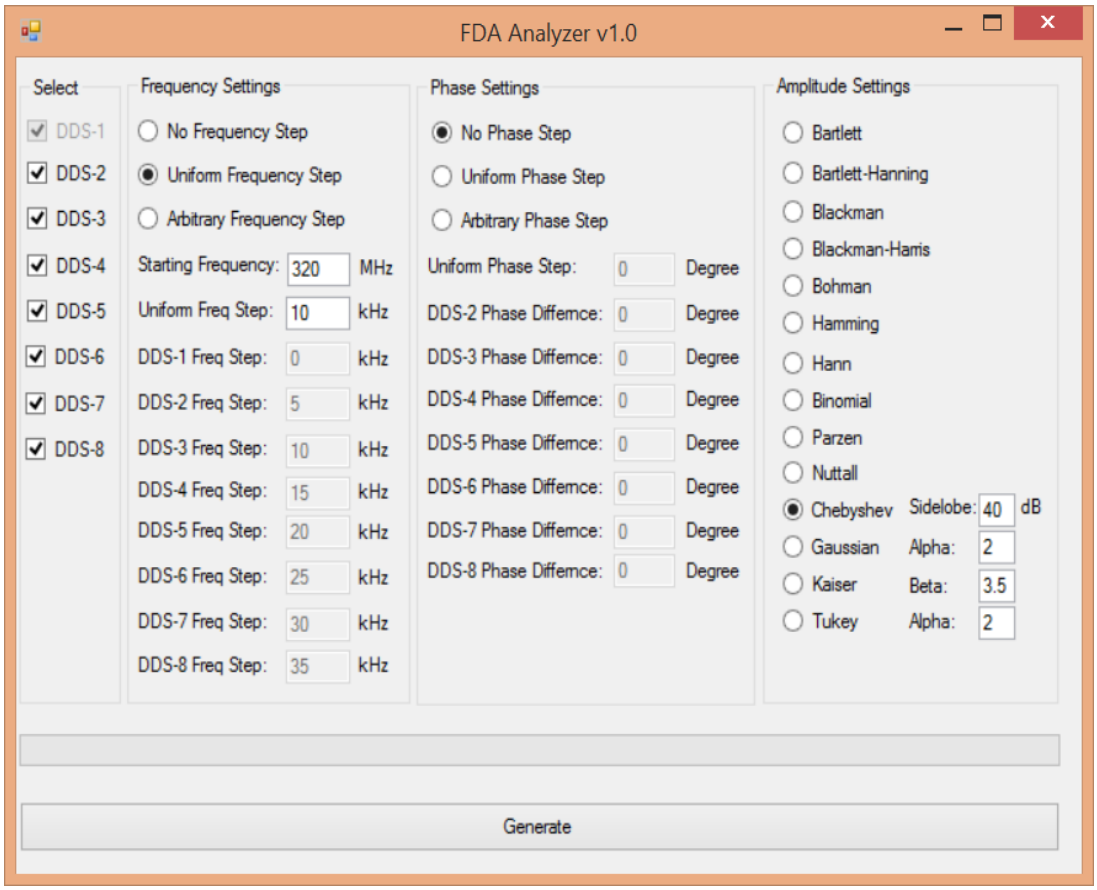

Figure 4.10 The User Interface for configuring the parameters of DDS

The interface permits the user to access to the three signal control parameters controlling the DDS. These are frequency, phase, and amplitude.

In the FDA Analyzer v1.0 software interface, the following options are available:

- ✓ **Select** - choose the DDS channels to be activated. DDS-1 is always selected due to multichip synchronization.

- ✓ **Frequency Settings-** configure the DDS Beamformer frequencies.

  - **No Frequency Step-** the frequencies of the selected DDSs are set to the starting frequency.

  - **Uniform Frequency Step-** configure DDS-1 at the starting frequency, the next DDS has a frequency offset, Δf, w.r.t. the previous DDS.

  - **Arbitrary Frequency Step-** When activated, all selected DDSs are configured with different frequencies according to the inputs.

- ✓ **Phase Settings-** configure the DDS Beamformer phases.

  - **No Phase Step-** All selected DDSs are set to zero phase offset.

  - **Uniform Phase Step-** configure DDS-1 at 0° phase offset, the next DDS has a phase offset, $\Delta\theta$, w.r.t. the previous DDS.

  - **Arbitrary Phase Step-** All selected DDSs are configured with different phase offsets according to the inputs.

- ✓ **Amplitude Settings-** choose a filter type for FDA beamformer amplitude distribution.

Software and hardware designed for the implementation of the DDS based FDA have been presented so far.

The cables which are used during the measurements are all standard length the phase balance. The other parts that are used in the measurements will be regarded as general parts and no further information will be provided about them.

4.4. Test Setups and Experiments

At the measurements two basic tests are performed in the laboratory without using any antenna. Firstly, DDS output frequency, phase, amplitude and spectral purity are measured by a digital oscilloscope and an RF Spectrum analyzer. Then, DDS based FDA beam-former output is measured by a Peak Power Analyzer with a peak power sensor and RF Spectrum Analyzer. The tests are presented together with the results in detail in the following sub-sections.

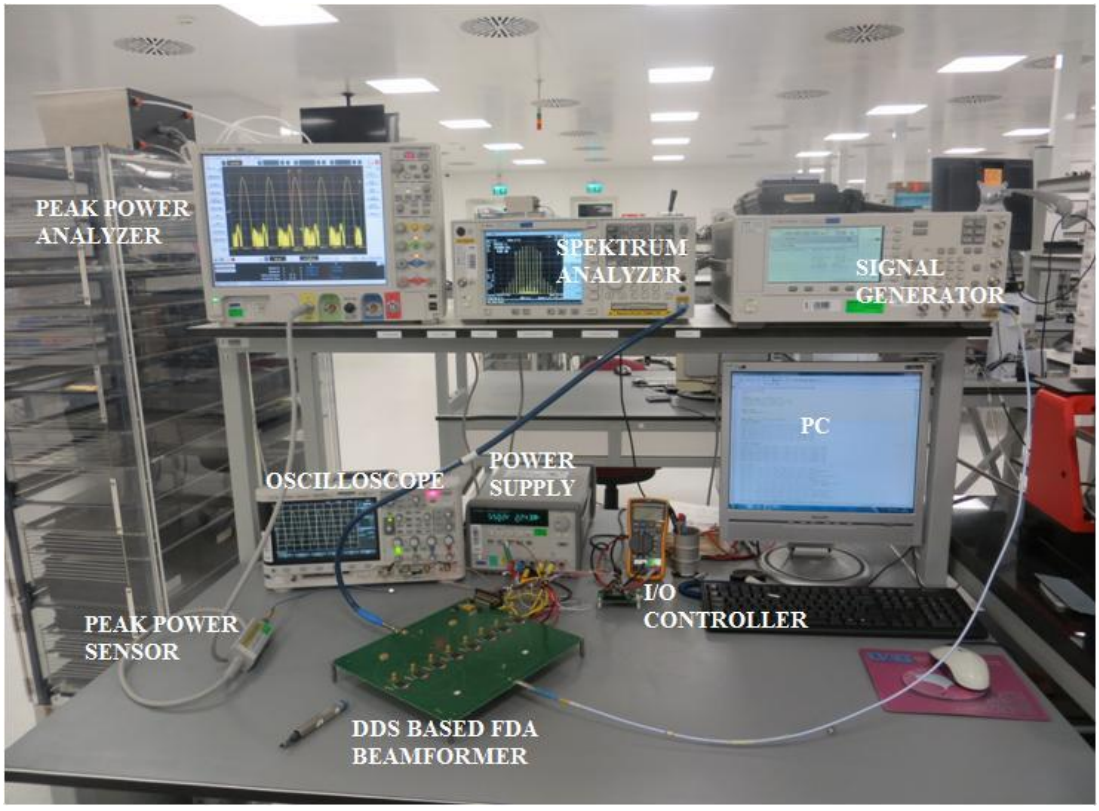

Figure 4.11: A photograph of the General Measurement Setup

The following is an outline of the equipment to be used for testing of the DUT (FDA-Based Beam-former).

Table 4.2: Equipment List

No	Item Name/Description	Part Number	Quantitiy
1	Signal Generator	Agilent/E8257D	1
2	Spectrum Analyzer	Agilent/N9030A	1
3	Power Supply	Agilent/E3631A	1
4	Power Meter	Agilent/8990B	1
5	Power Sensor	Agilent/N1924A	1
6	Oscilloscope	Agilent/DSO-X 3034A	1

4.4.1. Test Setup – 1

Frequency, phase, amplitude and spectral purity of DDS channels are measured by using laboratory tools and designed hardware in this test setup shown in Figure 4.12.

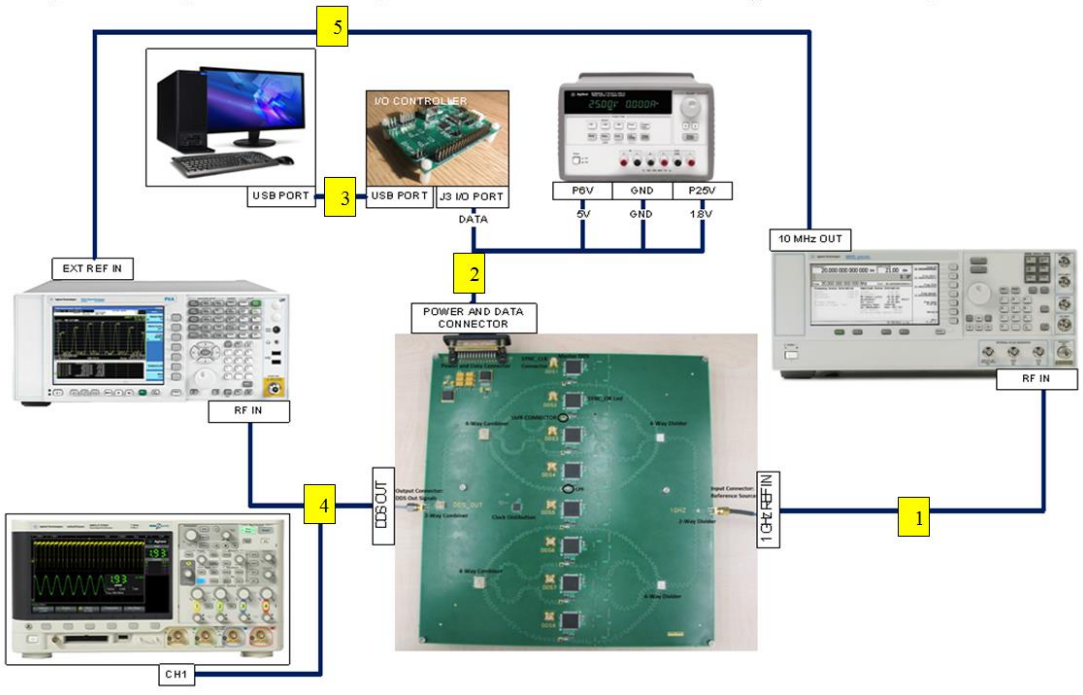

Figure 4.12: Configuration of Test Setup-1

Necessary hardware connections for Test Setup-1 are listed in Table 4.3. Connect the terminals listed under “From” column to the terminal listed under “To”, using the hardware listed under “With” column.

Table 4.3: Test Setup-1 Connections

<table>
<tr><th>No</th><th>From</th><th>To</th><th colspan="2">With</th></tr>
<tr><td>1</td><td>Signal Generator RF Out</td><td>DUT- 1GHz Connector</td><td colspan="2">SMA-SMA RF Cable</td></tr>
<tr><td rowspan="4">2</td><td>Power Supply P6V</td><td rowspan="4">DUT- Power and Data Connector</td><td rowspan="4">Power and Data Cable</td><td>5V Connector</td></tr>
<tr><td>Power Supply P25V</td><td>1.8V Connector</td></tr>
<tr><td>Power Supply GND</td><td>GND Connector</td></tr>
<tr><td>I/O Controller J3 I/O Connector</td><td>Data Connector</td></tr>
<tr><td>3</td><td>I/O Controller USB-Port</td><td>PC USB-Port</td><td colspan="2">USB-USB Cable</td></tr>
<tr><td rowspan="2">4</td><td>Spectrum Analyzer RF Input Connector</td><td rowspan="2">DUT- DDS Out Connector</td><td colspan="2">SMA-SMA RF Cable</td></tr>
<tr><td>or Oscilloscope CH1</td><td colspan="2">BNC-BNC RF Cable</td></tr>
<tr><td>5</td><td>Signal Generator 10MHz Out</td><td>Spectrum Analyzer Ext-Ref In</td><td colspan="2">BNC-BNC RF Cable</td></tr>
</table>

Note: 5VDC and 1.8VDC are applied to the DUT (DDS based FDA Beam-former). When only one DDS channel is active and DUT is excited by 1GHz Reference Source, 5VDC current limit is between 0.9A and 1.1A. Furthermore, 1.8VDC current limit is between 0.20A and 0.25A

Figure 4.12 illustrates that signal generator is used to excite the FDA beam forming network in this setup. By using FDA Analyzer user interface, only one DDS channel is activated, other channels are deactivated.

In this configuration, the aim is to ensure that each DDS channel generates a sinusoidal waveform at frequencies up to 400 MHz and that the relative phase and amplitude of the output signal of each DDS channel can be controlled. The results show that the expected behavior is achieved.

Figure 4.13 demonstrates a photograph of the setup which is based on the setup shown in Figure 4.12.

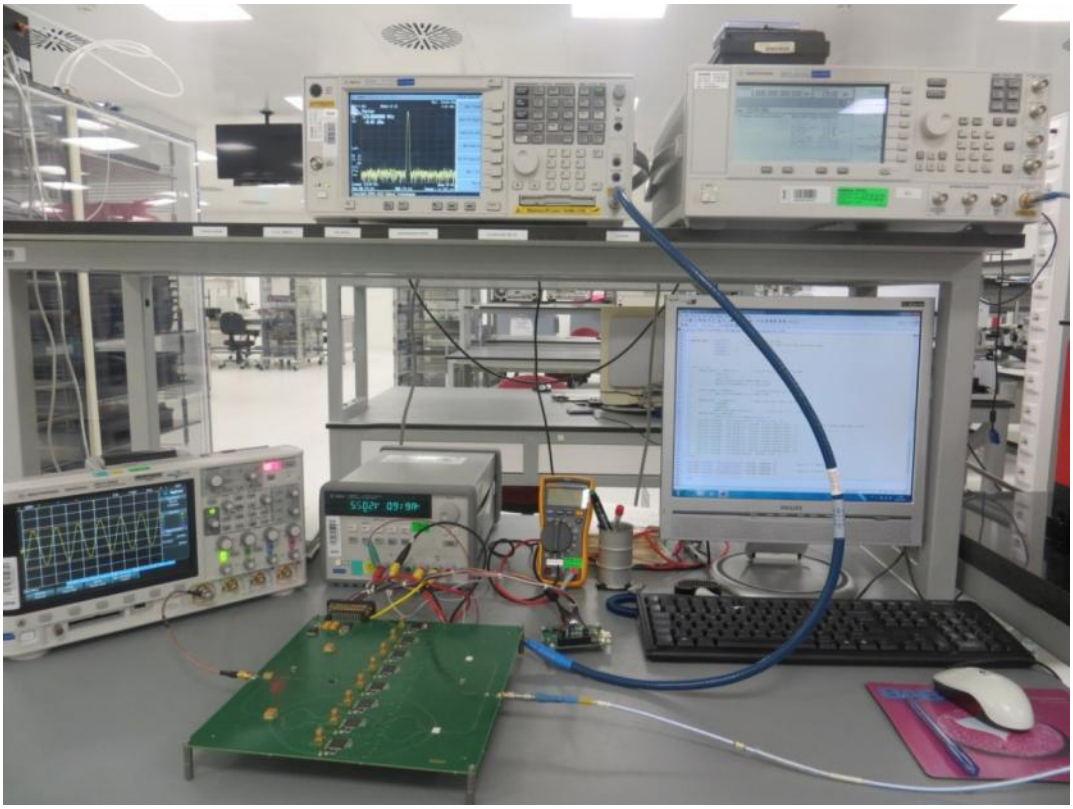

Figure 4.13: A photograph of the measurement setup-1

4.4.1.1. Experiment with Test Setup- 1

The main aim is to verify that the DDS is capable of generating agile sinusoidal waveforms of different frequencies in this configuration. The first result is shown in Figure 4.14 as a demonstration.

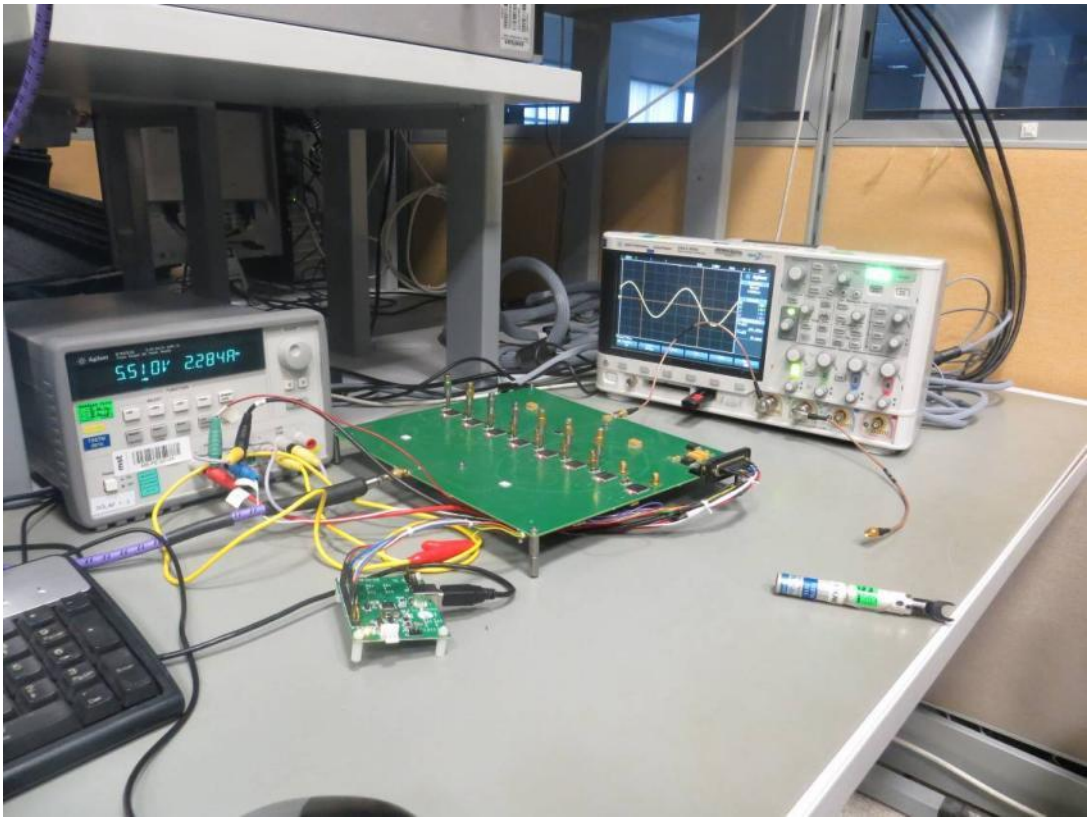

Figure 4.14: Sinusoidal waveform on the oscilloscope screen

By changing the frequency value in the user interface, the frequency synthesizer gives outputs of different frequencies. As shown in Figure 4.15, DDS generates perfect signals at 100MHz and 320MHz frequencies.

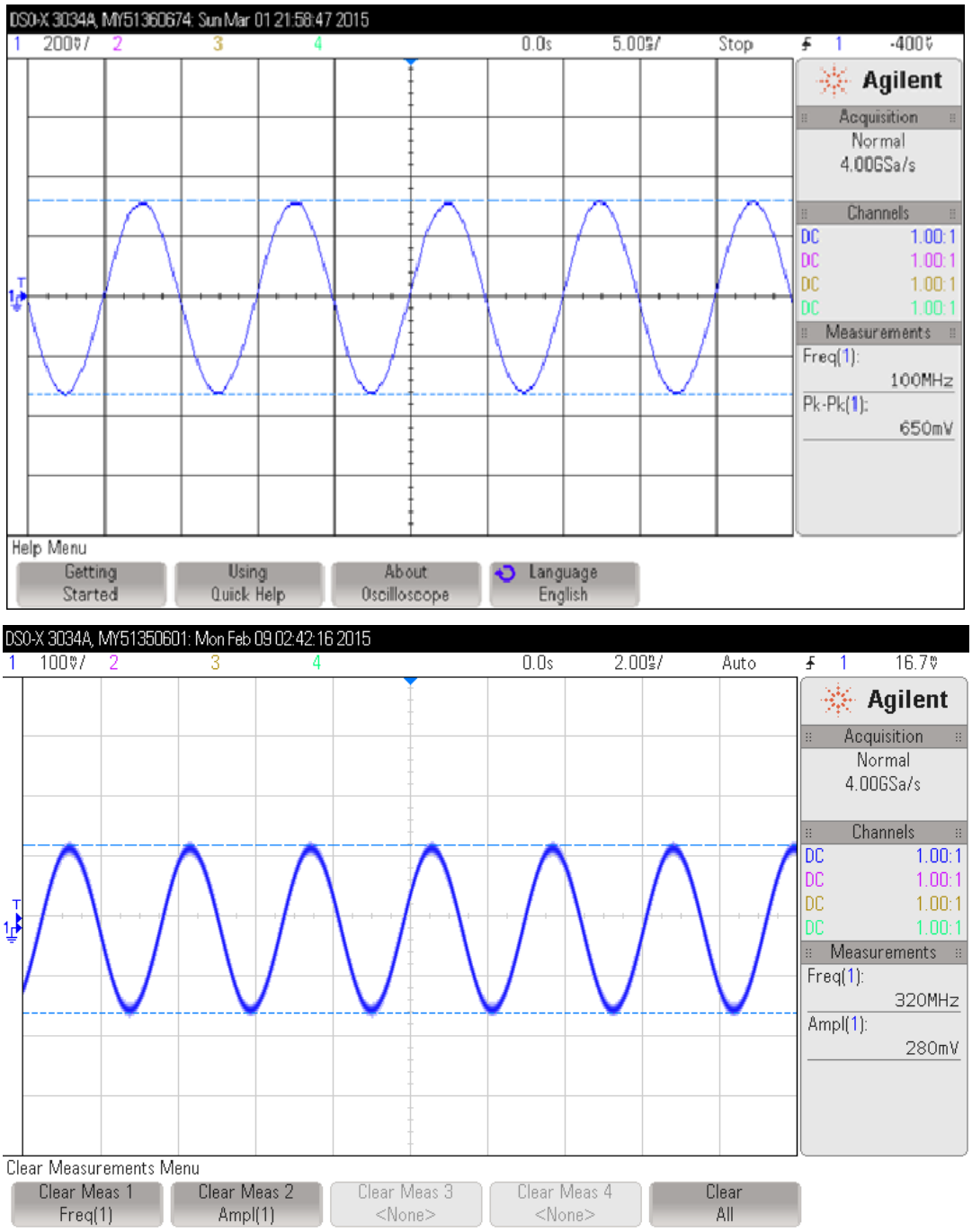

Figure 4.15: DDS Output Waveforms @100MHz and 320 MHz

DDS outputs have good spectral purity as shown Figure 4.16 . Spur Free Dynamic Range is about 75dB at 1 MHz span.

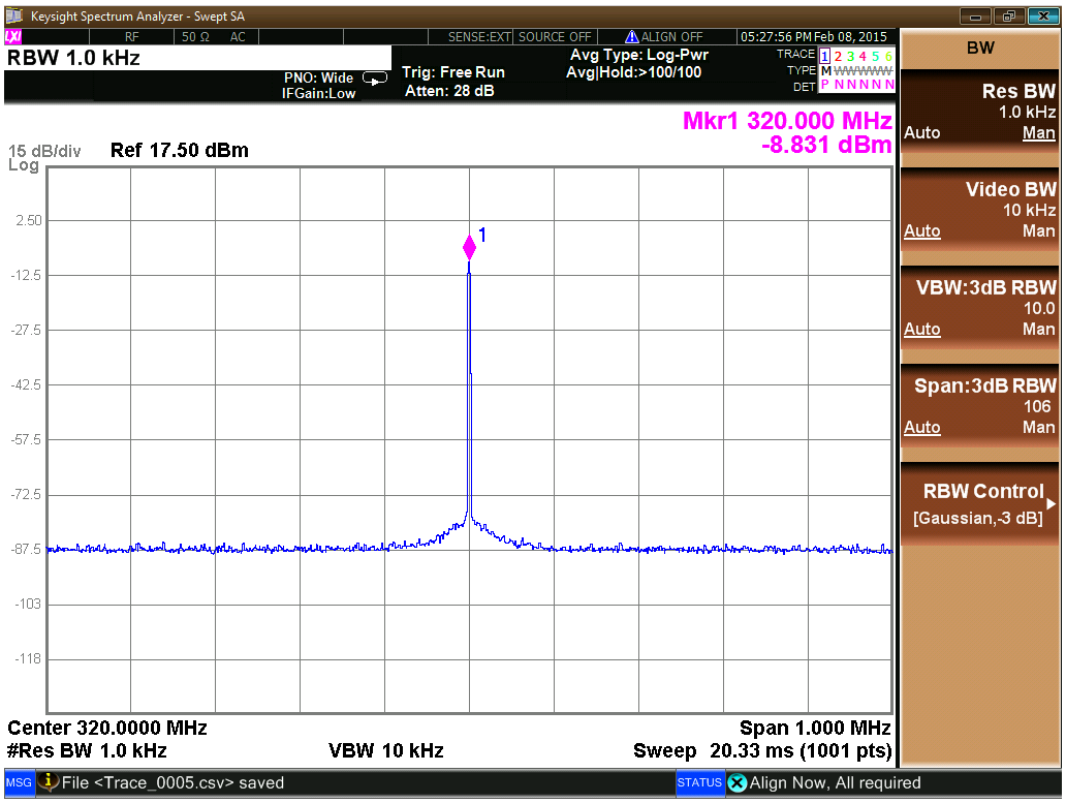

Figure 4.16: The spectral purity of the AD9910 DDS at 320 MHz

Since the oscilloscope cannot precisely measure the frequency, the small frequency increments on the carrier signal that is generated by DDS can accurately be measured by means of an RF Spectrum Analyzer as shown in Figure 4.17. In this figure, 10kHz frequency offset on the 320MHz carrier signal which adds up to 320.010MHz can be clearly observed.

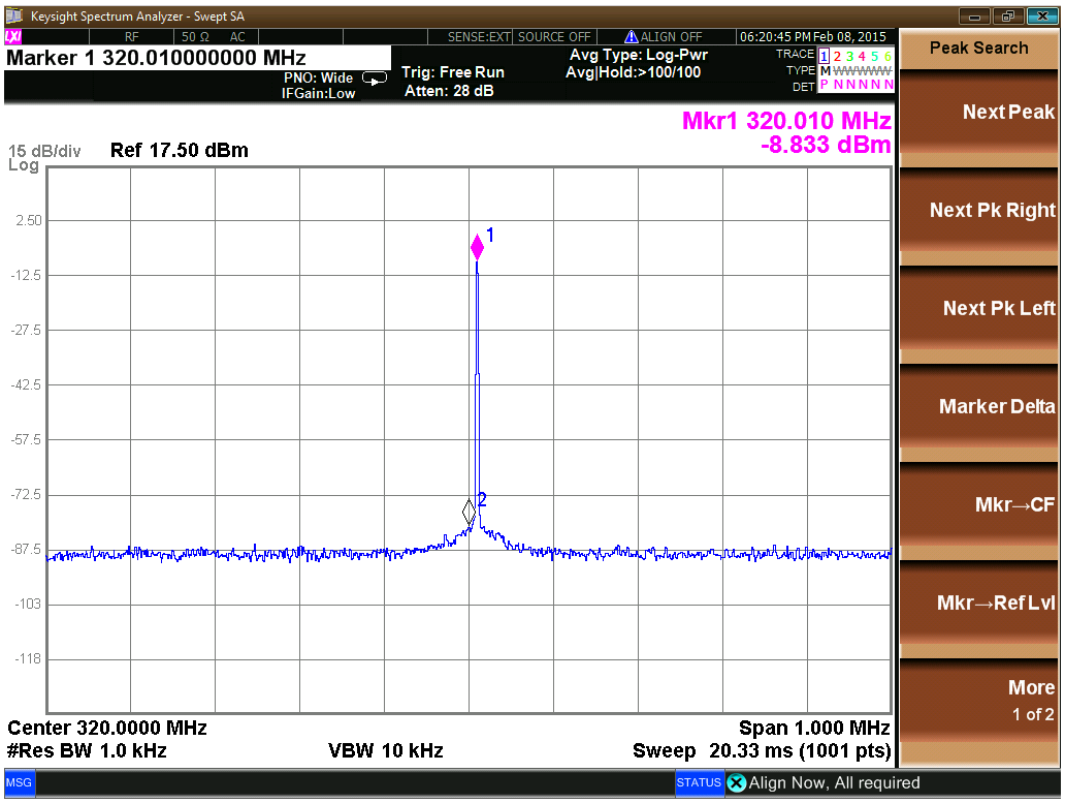

Figure 4.17: Frequency Step:10kHz @320MHz is shown here

Frequency diverse signals should have 0° phase at t = 0. If the Auto Clear Phase Accumulator bit of the DDS Control Function Register is set to 1, the phase accumulator is reset by the DDS synchronously whenever there is an I/O_UPDATE or a profile change. In this way, phase synchronization is achieved among the frequency diverse signals as shown in Figure 4.18.

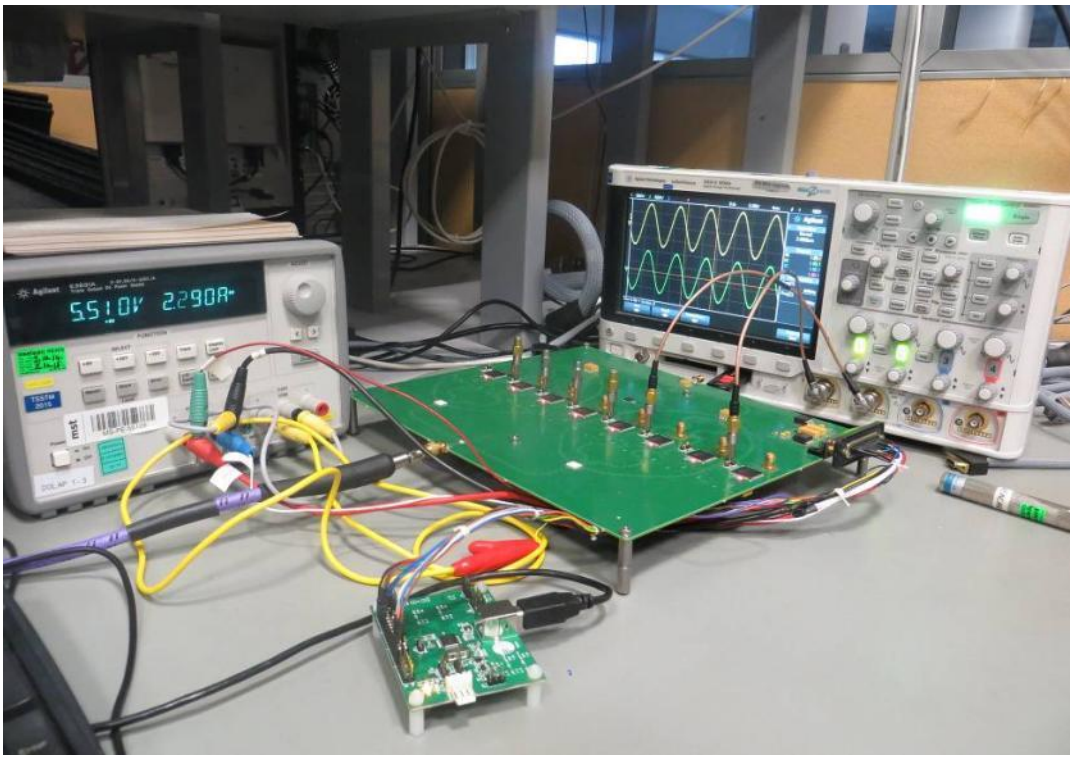

Figure 4.18: Phase Synchronization Measurement Test Setup

When DDS channels are synchronous, the frequencies and phases of the two signals become the same. In Figure 4.19, the resulting waveforms after phase and frequency synchronization among two DDS channels are shown.

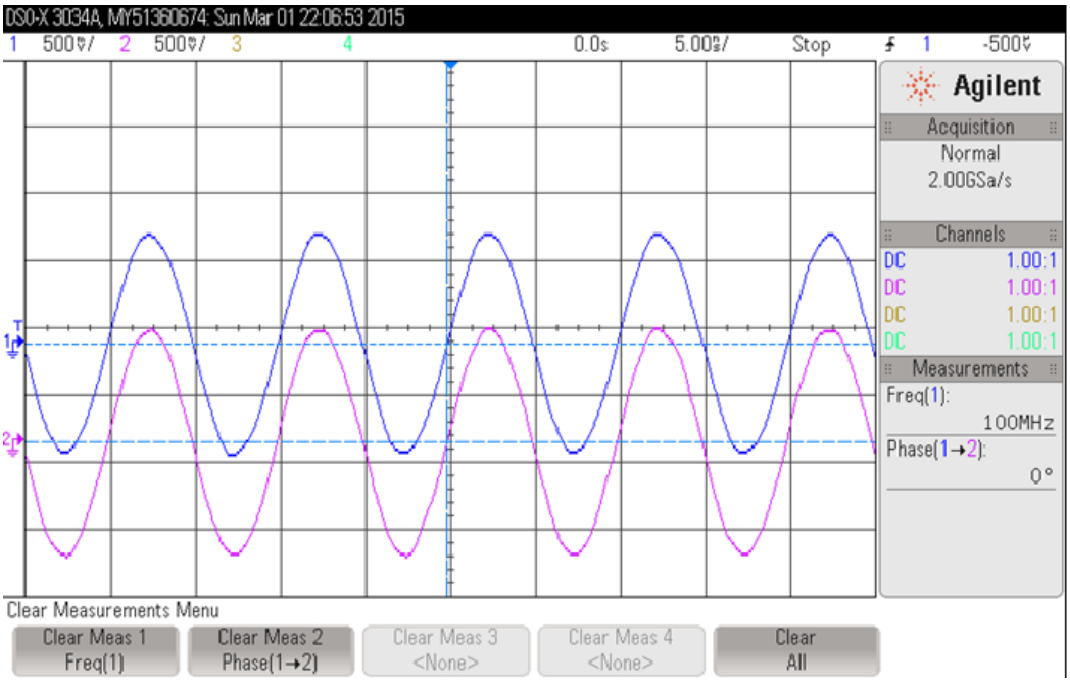

Figure 4.19: Phase Synchronization between DDS-1 and DDS-2

The differences in the phase between consecutive DDS channels may cause deviation to phase synchronization, which in turn changes the shape of the radiation pattern. The solution to this problem is applying phase offset among DDS channels. A 16-bit phase offset word (POW) can digitally control the relative phase of the DDS signal. In Figure 4.20, the resulting waveforms by applying 90° and 180° phase offset among DDS-1 and DDS-2 are shown.

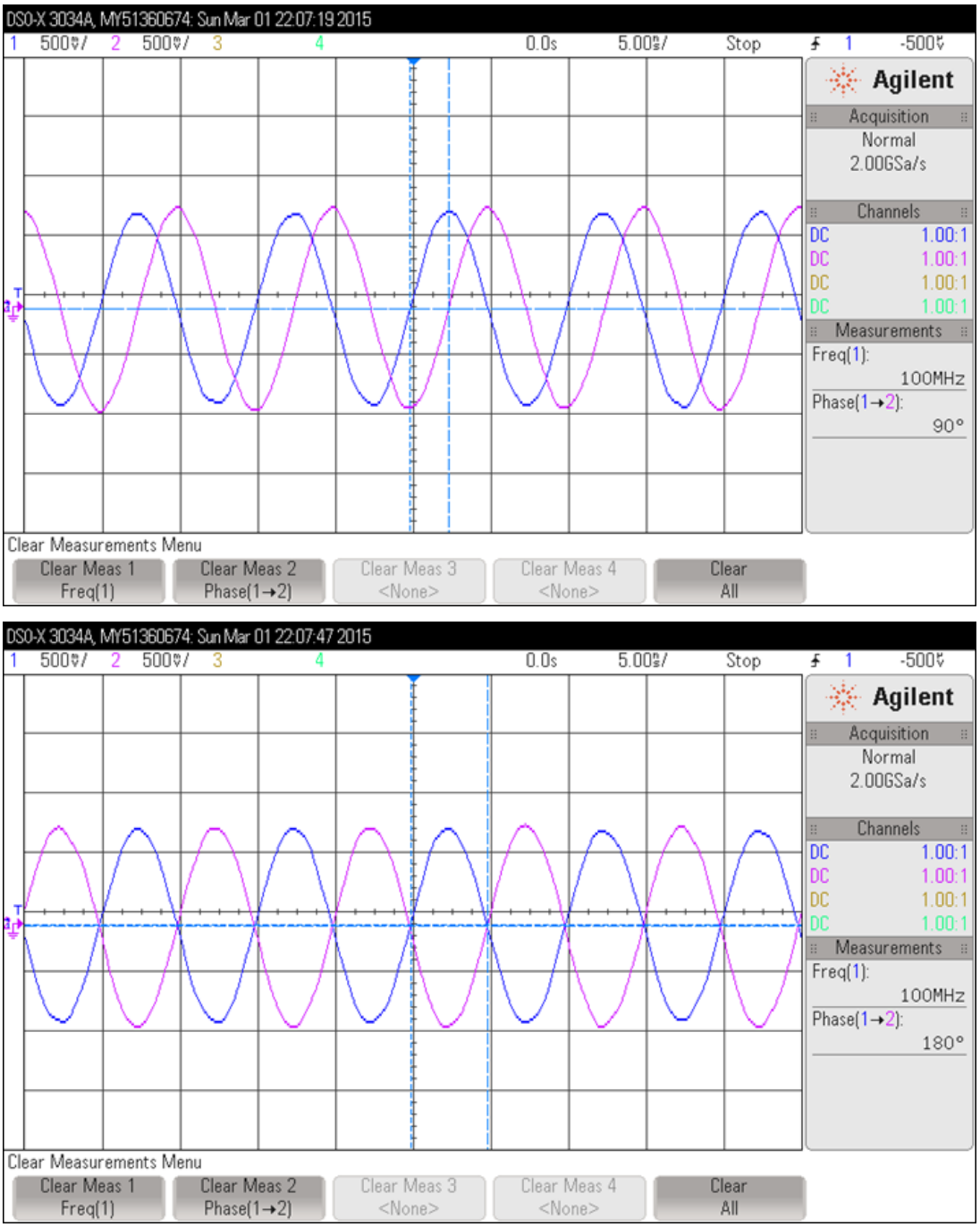

Figure 4.20: 90° and 180° Phase offset between DDS-1 and DDS-2

Amplitude distribution across the aperture of the array plays a crucial role in forming the beam shape. It is possible to change the relative amplitude of the DDS output signal via a 14-bit amplitude scale factor (ASF).

The amplitude scale is as shown

$$AmplitudeScale = \frac{ASF}{2^{14}} \tag{4.1}$$

$$AmplitudeScale = 20\log\left(\frac{ASF}{2^{14}}\right)$$

where the amplitude is represented as a fraction of full scale and the lower quantity represented by decibels relative to full scale. In Figure 4.21, the resulting waveforms by applying 0.5 amplitude scale value between DDS-1 and DDS-2 channels are shown. It is clearly seen that amplitude level decreases with an amplitude scale ratio.

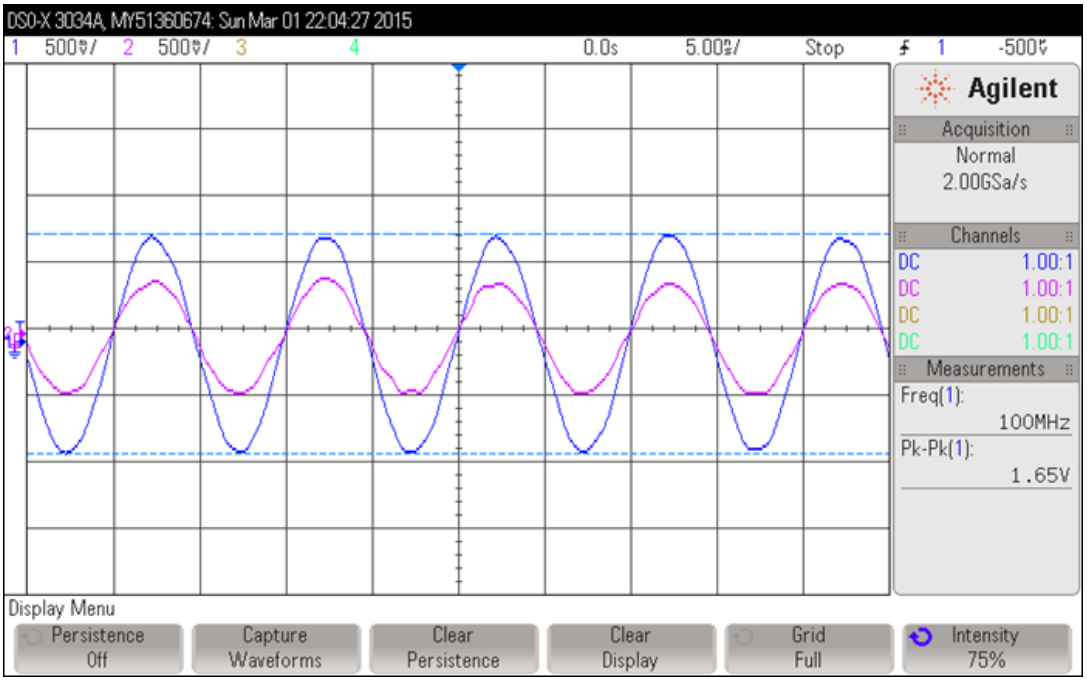

Figure 4.21:Amplitude Scale Factor 0.5 between DDS-1 and DDS-2

So far, we have conducted experiments showing that the DDS channels present on the designed board can be independently configured to achieve the desired output.

4.4.2. Test Setup-2

The main goal is to check the FDA concept by using the hardware, software and laboratory equipment in this test setup. However, any antenna is not used and measurement isn't performed in an anechoic chamber. Figure 4.12 and Figure 4.13 show the equipment utilized in the new test configuration together with the peak power analyzer and its power sensor. Figure 4.22 illustrates the configuration for this setup.

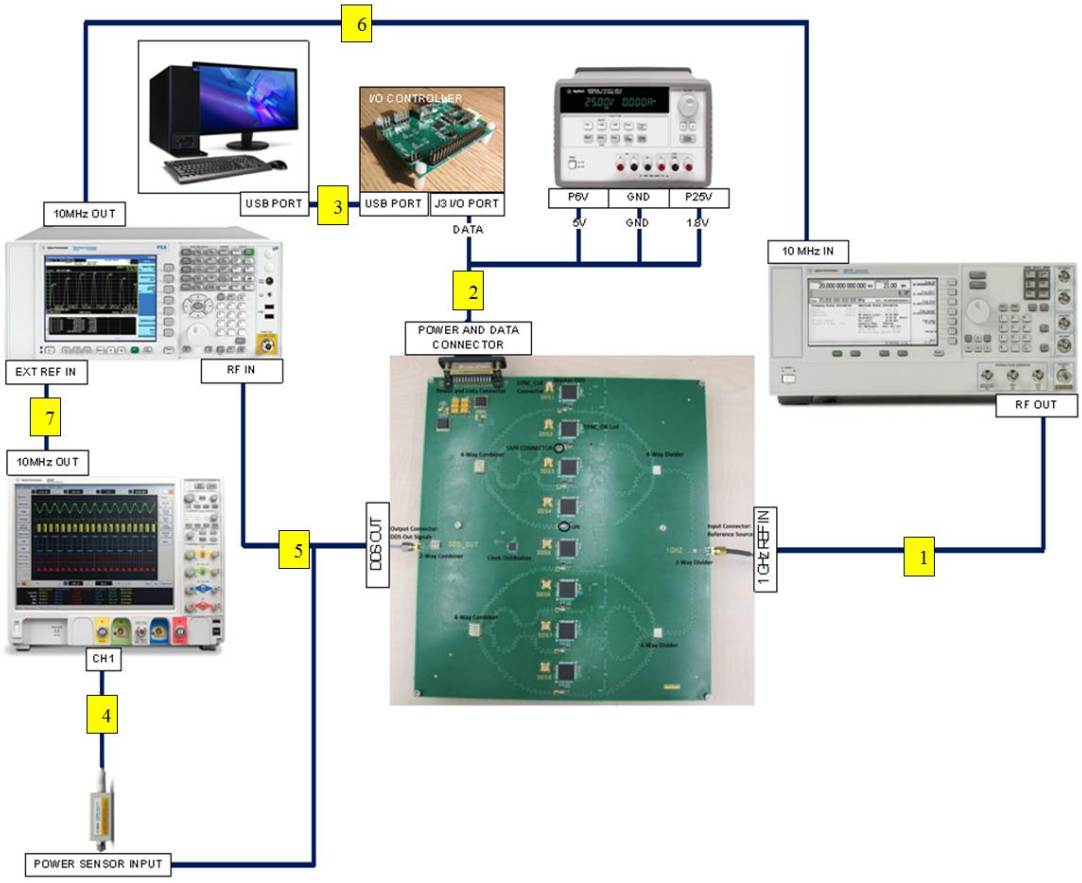

Figure 4.22: Configuration of Test Setup-2

Necessary hardware connections for Test Setup-2 are listed in Table 4.4. Connect the terminals listed under "From" column to the terminal listed under "To", using the hardware listed under "With" column.

Table 4.4: Test Setup-2 Connections

No	From	To	With	
1	Signal Generator RF Out	DUT- 1GHz Connector	SMA-SMA RF Cable	
2	Power Supply P6V	DUT- Power and Data Connector	Power and Data Cable	5V Connector
	Power Supply P25V			1.8V Connector
	Power Supply GND			GND Connector
	I/O Controller J3 I/O Connector			Data Connector
3	I/O Controller USB-Port	PC USB-Port	USB-USB Cable	
4	Power Meter CH1	Power Sensor Data Connector	Power Sensor Data Cable	
5	Spectrum Analyzer RF Input Connector	DUT- DDS Out Connector	SMA-SMA RF Cable	
	or Power Sensor Input Connector		BNC-BNC RF Cable	
6	Signal Generator 10MHz In	Spectrum Analyzer 10MHz Out	BNC-BNC RF Cable	
7	Spectrum Analyzer Ext-Ref In	Power Meter 10MHz Out	BNC-BNC RF Cable	

Note: 5VDC and 1.8VDC are applied to the DUT (DDS based FDA Beam-former). When only one DDS channel is active and DUT is excited by 1GHz Reference Source, 5VDC current value must be between 2.2A and 2.4A. Furthermore, 1.8VDC current value must be between 0.35A and 0.4A

In this setup, signal generator is used to excite to FDA beam forming network. The outputs of the DDSs are transferred to the beam-former network's 4-way equal combiners and summed at the common port of the beam-former network's 2-way equal combiner. Finally, the sum is fed to the detector which is Agilent N1924A power sensor. The sensor is then connected to a peak power analyzer for inspection of the output waveform of the DDS based beam-former network.

This configuration aims to get the beam-former to work like an FDA steering to broadside only. The waves propagate through the lines and interference is seen at the output port of the combiner. Although the range of interference point to the array origin is not at the far-field of the array, the experimental results are compatible with the outcomes of the simulations because the array is set to steer to the broadside direction.

Figure 4.23 demonstrates a photograph of the setup which is based on the setup shown in Figure 4.22.

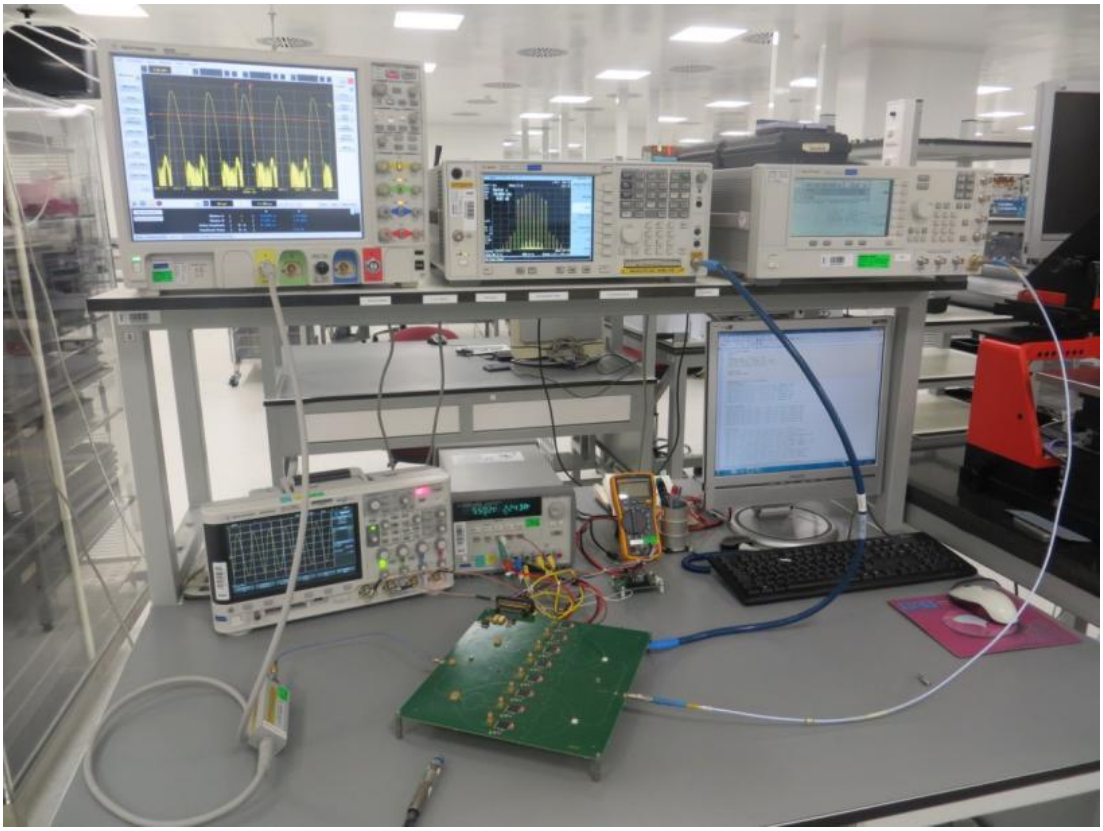

Figure 4.23: A photograph of the Test Setup-2

4.4.2.1. Experiments with Test Setup-2

This section focuses on three measurements for the justification of the findings. Most of the measurements are used for demonstration of the DDS based FDA Beam-former concept, so they will not be explained in details.

4.4.2.1.01. Experiment- 1

In this measurement, the aim is to observe the amplitude modulation at the output of the designed DDS based FDA Beam-former network. In fact, the results are satisfactory regarding in terms of the modulation. The first result is demonstrated in Figure 4.24. Even though the waveform is not a perfect $\sin(N\varphi)/\sin(\varphi)$ owing to imperfections in the utilized devices, the amplitude modulation in time is obvious [16].

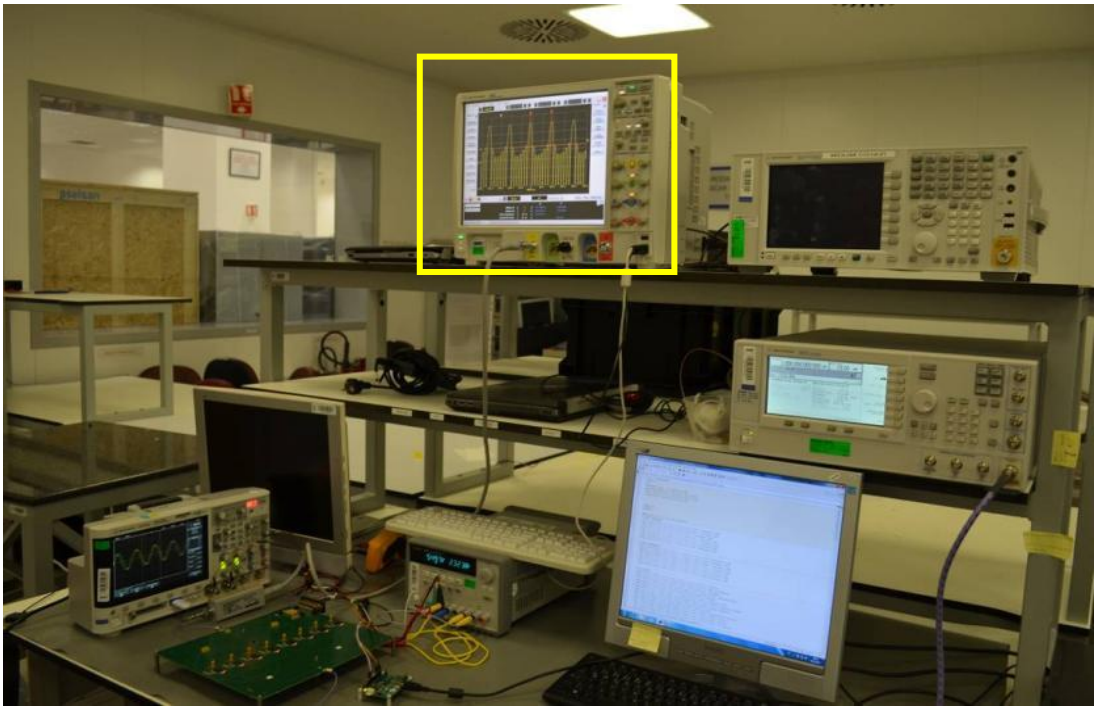

Figure 4.24: AM observation of FDA on the PPA screen

Sample measurement and simulation results for the second configuration are generated from the parameters shown in Table 4.5. According to the table, 320MHz start frequency and 10 kHz step frequency are selected to generate signals from DDSs. There is no amplitude distribution filter in this measurement. The frequency difference between the elements is determined to be 10 kHz and the corresponding beam period is 100us.

The range period is 300km and the null to null beam-width is calculated to be 25us, since all measurements are supposed to be performed for $\theta = 0^o$. The simulation of this configuration is illustrated in Figure 4.25 and the result of the measurement is illustrated in Figure 4.26.

Table 4.5: Parameters of Experiment-1 configuration

Parameters	Measured	Calculated/Simulated
Frequency Start (MHz)	320	320
Frequency Step (kHz)	10	10
Beam Period (us)	99.92	100
Amplitude Distribution Filter	-	-
Phase Offset (°)	0	0
Amplitude (dBm)	9.7	-
Beam Width (us)	11.2	10.5
Side Lobe Level (dB)	12.1	14.7
Null to Null interval (us)	25,78	25

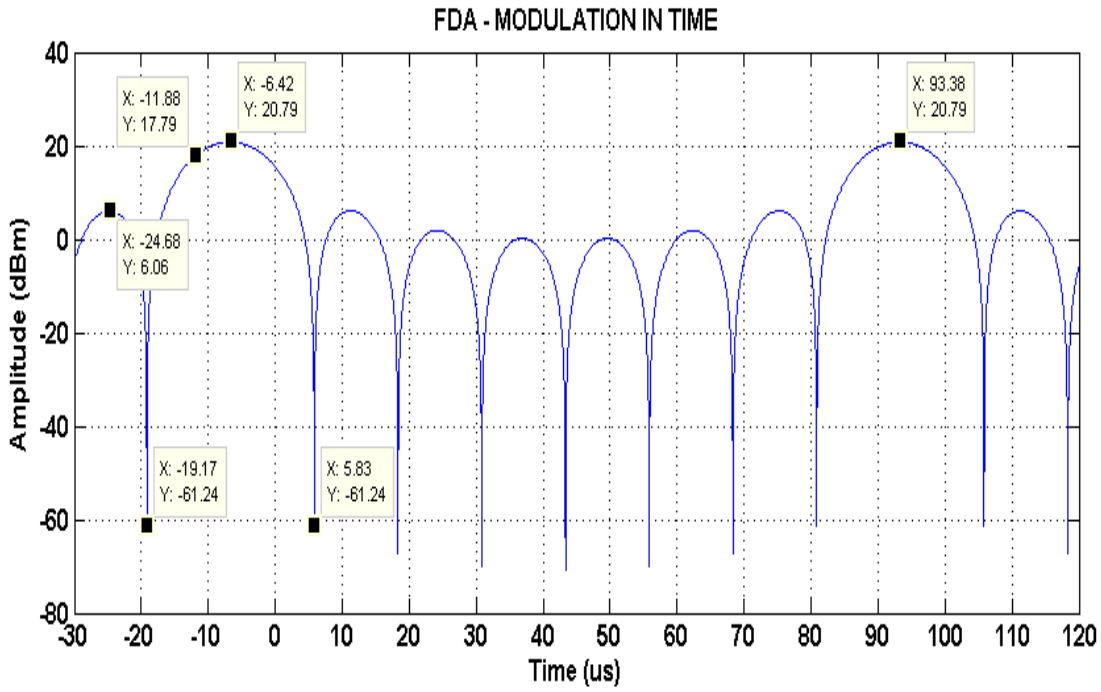

Figure 4.25: The simulation result for the parameters in Table 4.5

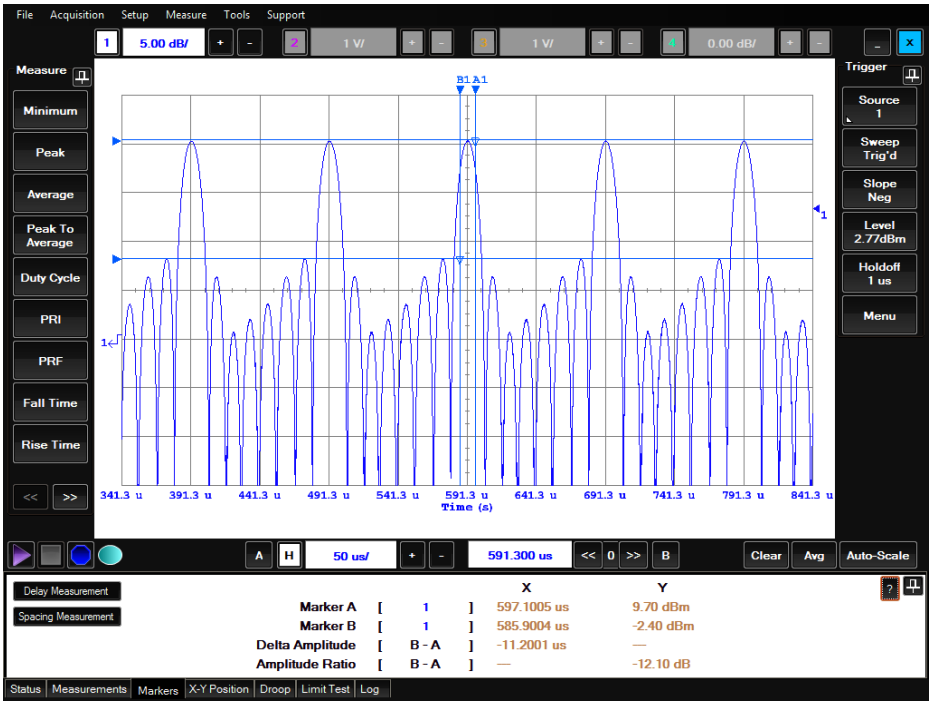

Figure 4.26: The output waveform of beam-former on the PPA screen

The null-to-null beam-width of the measurement result is 25.78us as shown in Figure 4.27, which is almost the same as with the value shown in Table 4.5.

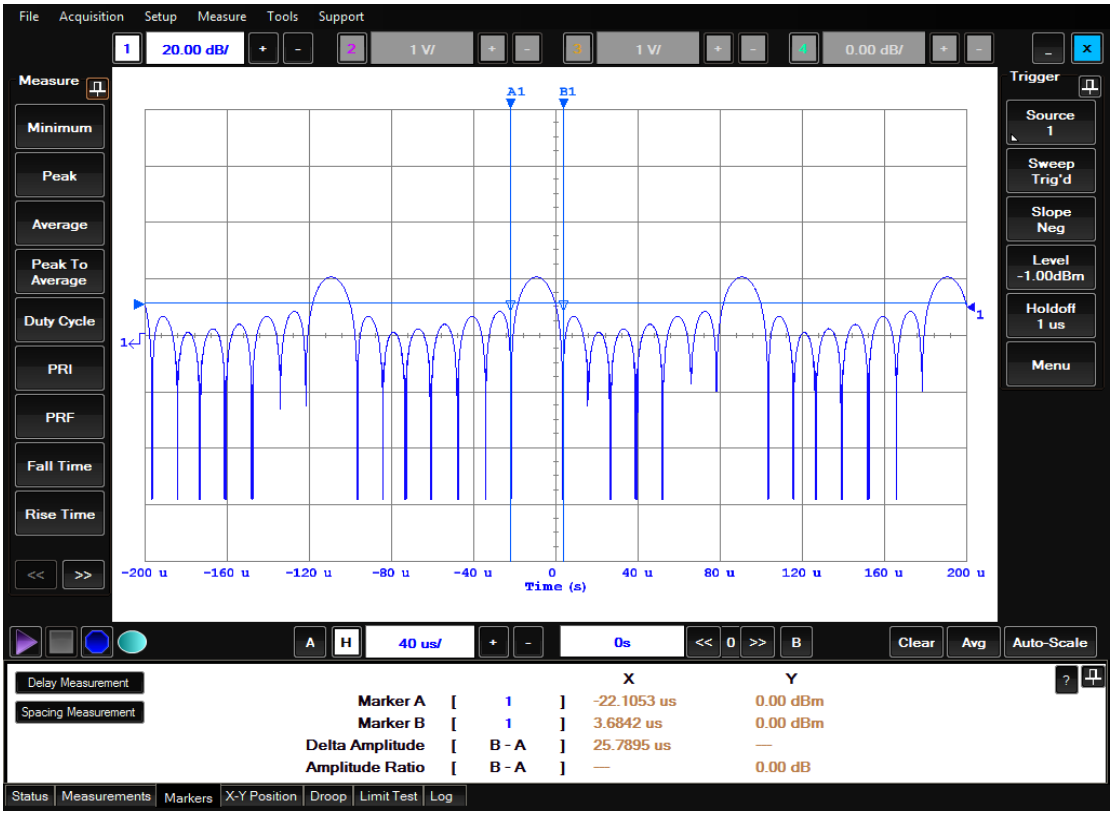

Figure 4.27:Null to Null Beam-width Measurement

The beam period is measured to be 100us, consistent with the calculated value as shown in Figure 4.25.

4.1.1.1.01. Experiment-2

Table 4.6 demonstrates the parameters for this measurement. Only frequency step parameter is different from Table 4.5.

Table 4.6: Parameters of Experiment-2 configuration

Parameters	Measured	Calculated/Simulated
Frequency Start (MHz)	320	320
Frequency Step (kHz)	15	15
Beam Period (us)	66.65	66,67
Amplitude Distribution Filter	-	-
Phase Offset (°)	0	0
Amplitude (dBm)	10.4	20.79
Beam Width (us)	7.5	7
Side Lobe Level (dB)	12.4	14.7
Null to Null interval (us)	16,32	16,67

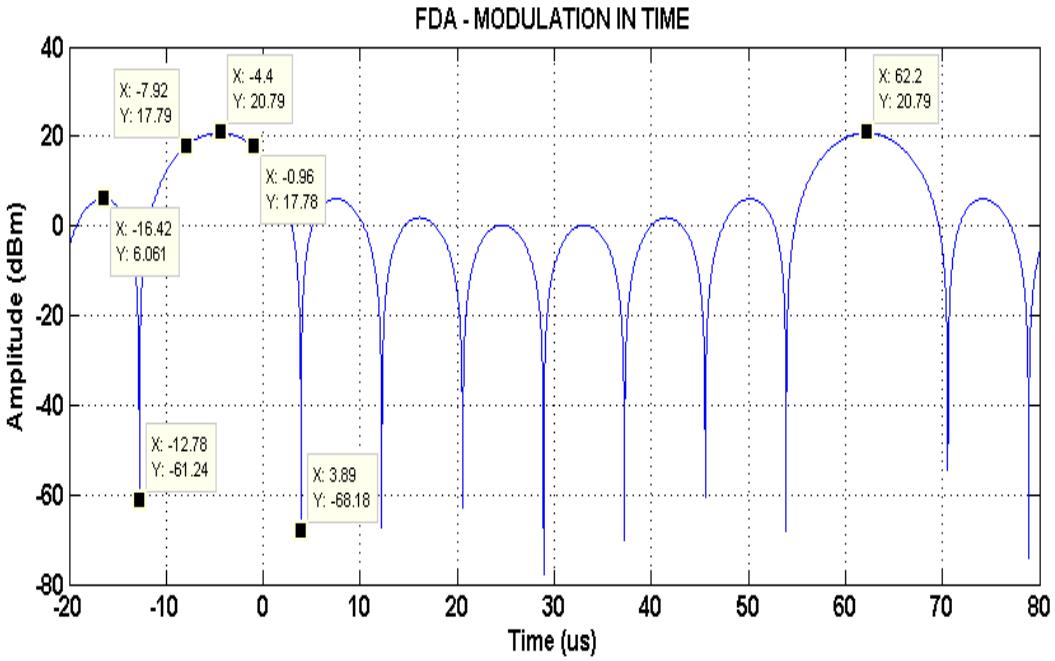

Figure 4.28: The simulation result for the parameters in Table 4.6

Figure 4.29: The output waveform of beam-former on the PPA screen

The uniform amplitude distribution on the outputs of DDS based FDA beam-former is measured by using spectrum analyzer as shown in Figure 4.30.

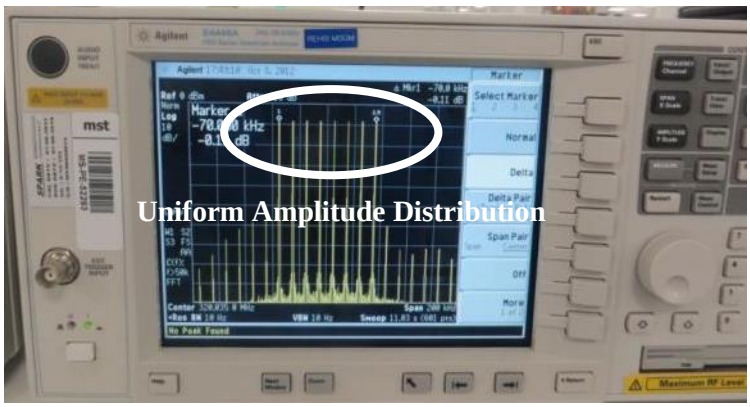

Figure 4.30:The output waveform of beam-former on the SA screen

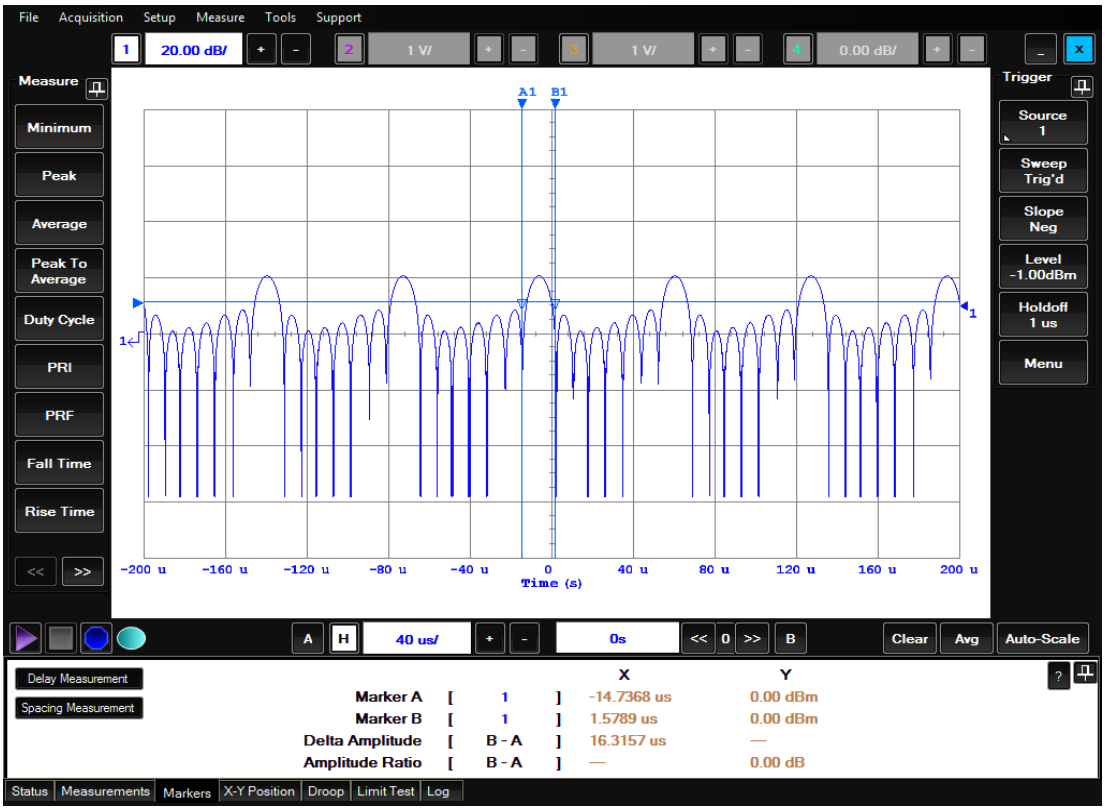

Figure 4.31:Null to Null Beam-width Measurement

Comparing the results, we can see that the calculated outcomes are in very good agreement with the ones that are obtained from this measurement.

In addition, if we compare the results of the previous section with the ones obtained in this part, we can conclude that, as the frequency step increases, the beam period, the beam width, the range period and the null to null interval decreases. This feature is one of the key benefits of using the DDS based FDA beam-former, that is, one can dynamically change important parameters like the beam period, the beam width etc. of the array as fast as the DDS switching time and without having to alter the hardware as in the case where true delay lines are used to construct the FDA beam-former.

4.1.1.1.02. Experiment-3

The side lobe levels in uniform amplitude tapering of a ratio unity and non-uniform amplitude tapering such as Hamming, Binomials, Blackman, Chebyshev, Hann etc. are analyzed in this measurement. Side lobe level for uniform amplitude distribution is measured about -12dBc in the previous measurement. Several non-uniform amplitude distributions are implemented in order to reduce the side lobe level. The side lobe level and beam width parameters are analyzed for different kinds of edge tapering distributions for two start frequencies and two frequency steps as shown in Table 4.7.

Table 4.7: Different kinds of edge tapering system SLL(dB) and BW(us) values

Filter TypeType	f=200MHZ Δf=10kHz		f=200MHZ Δf=15kHz		f=320MHZ Δf=10kHz		f=320MHZ Δf=15kHz	
	BW	SLL	BW	SLL	BW	SLL	BW	SLL
Bartlett	18,84	22,50	12,48	22,90	19,04	21,60	12,63	21,40
Bartlett-Hanning	20,33	25,50	13,43	25,90	20,45	25,70	13,40	26,00
Blackman	23,80	25,30	15,80	24,50	23,80	25,10	15,80	25,90
Blackman-Harris	27,80	22,50	18,24	23,50	27,75	24,10	18,43	23,50
Bohman	24,65	25,00	16,40	24,60	24,60	25,40	16,34	24,60
Chebyshev 40dB	15,93	27,50	10,60	27,70	16,55	24,40	10,62	24,60
Gaussian Alpha=2	16,23	25,90	10,64	25,90	16,17	25,90	10,79	25,60
Hamming	17,96	25,70	11,80	26,80	17,72	26,30	11,94	26,80
Hann	20,82	24,70	13,73	25,20	20,80	24,60	13,72	25,70
Kaiser Beta=3.5	16,05	26,20	10,46	26,30	16	25,6	10,4	26,1
Nuttall	20,56	23,90	18,01	23,70	27	22,2	18	22,2
Parzen	23,02	25,30	15,31	25,1	23,2	23,6	15,4	25,1
Triangular	15,9	23,8	10,5	23,9	16	21,5	10,6	22
Tukey Alpha=0.45	16,05	13,7	10,8	13,6	16,2	13,2	10,7	13,2
Tukey Alpha=2	20,8	25	13,77	25	21	23,2	13,8	23,3

The optimum beam width for a specified side lobe level is provided by Chebyshev distribution when the number of elements are limited. Since the element number of our DDS based FDA beamformer is fixed (N=8), Chebyshev is the optimum distribution for our case. To determine the optimum Chebyshev distribution, beam width, side lobe level, beam peak values are measured for two start frequencies and two frequency steps as shown in Table 4.8. According to Table 4.8, 40dB Chebyshev is the optimum filtering edge. If we want to increase the side lobe level suppression, i.e. 100dB SLL Chebyshev, the radiated peak power essentially drops because some of the corner elements become effectively turned off. On the other hand, if we want to keep the radiated power at the maximum level, then we will face with large side lobe levels which are also unwanted. Hence, we understand that there is a trade-off in this situation and that the optimum Chebyshev SLL suppression is 40dB which provides side lobe level suppression and keeps the reduction of the radiated power in an acceptable level.

Table 4.8: Chebyshev's SLL, BW and Beam Peak values

Filter	Frequency	Step	BW(us)	SLL(dB)	Peak
Chebyshev_100dB	320MHz	10kHz	19.2us	26.7dB	3.2dB
Chebyshev_80dB			19.2us	25.5dB	3.4dB
Chebyshev_60dB			17.8us	25.3dB	3.9dB
Chebyshev_40dB			15.8us	24.9dB	4.9dB
Chebyshev_35dB			14.7us	23.7dB	5.3dB
Chebyshev_30dB			14.3us	21.9dB	5.9dB
Chebyshev_20dB			12.7us	16.8dB	7.4dB
Chebyshev_100dB	200MHz	10kHz	19.2us	26.7dB	3.2dB
Chebyshev_80dB			19us	25.5dB	3.4dB
Chebyshev_60dB			18us	25.1dB	3.95dB
Chebyshev_40dB			16us	24.3dB	4.9dB
Chebyshev_35dB			14.7us	23.3dB	5.26dB
Chebyshev_30dB			14.45us	21.8dB	5.81dB
Chebyshev_20dB			12.35us	16.7dB	7.49dB

Table 4.9: Parameters of Experiment-3 configuration

Parameters	Measured	Calculated/Simulated
Frequency Start (MHz)	320	320
Frequency Step (kHz)	10	10
Beam Period (us)	100	100
Amplitude Distribution Filter	Chebyshev(40dB)	Chebyshev(40dB)
Phase Offset (°)	0	0
Amplitude (dBm)	4.9	15.35
Beam Width (us)	15.8	14.7
Side Lobe Level (dB)	24.9	45
Null to Null interval (us)	48	45.9

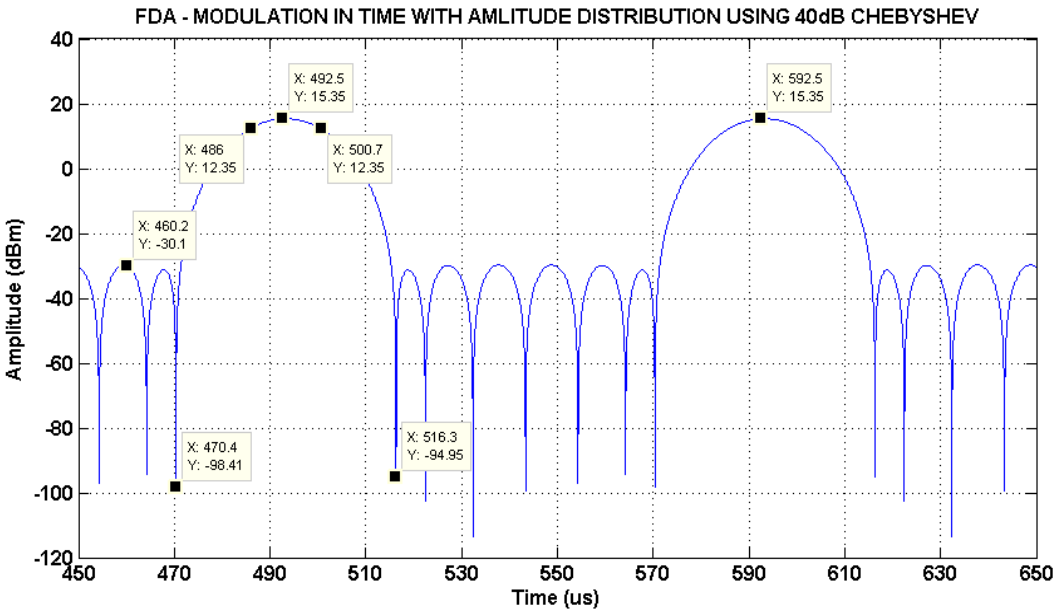

Figure 4.32: The Simulation Waveform for the parameters in Table 4.9

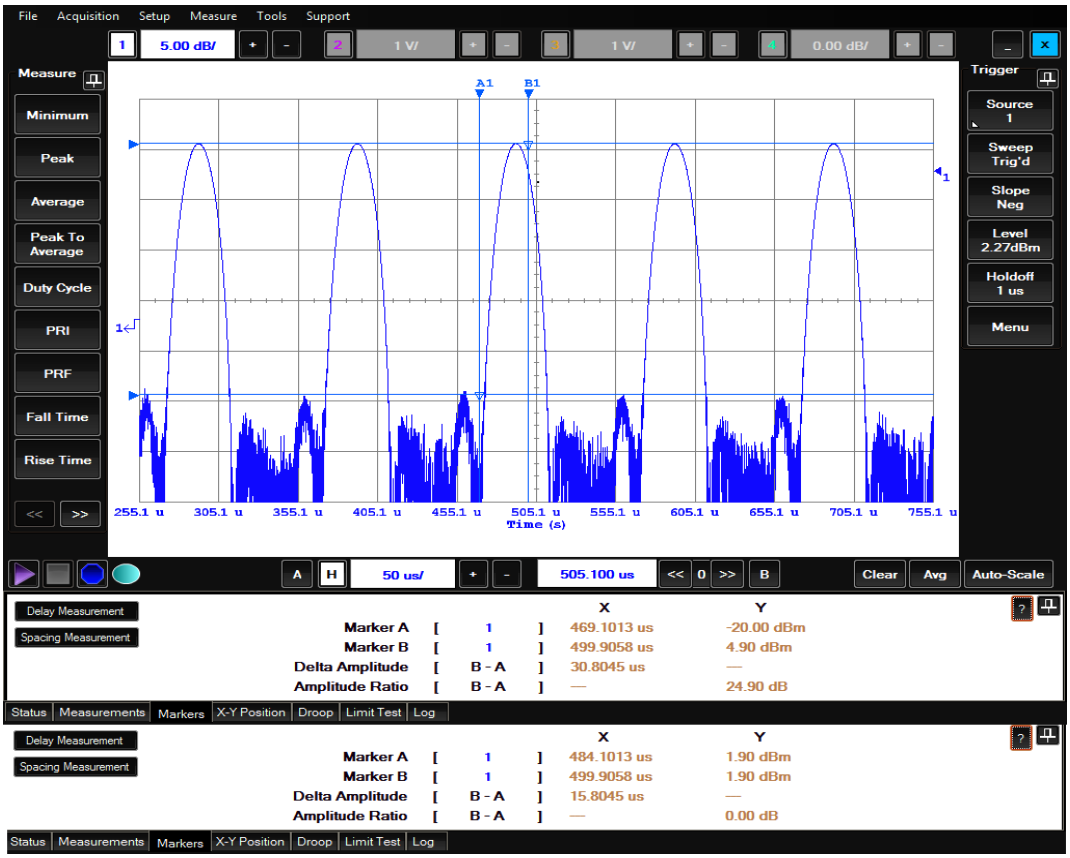

Figure 4.33: The output waveform of beam-former on the PPA screen

The 40dB Chebyshev amplitude distribution on the outputs of DDS based FDA beam-former is measured by using spectrum analyzer shown in Figure 4.34

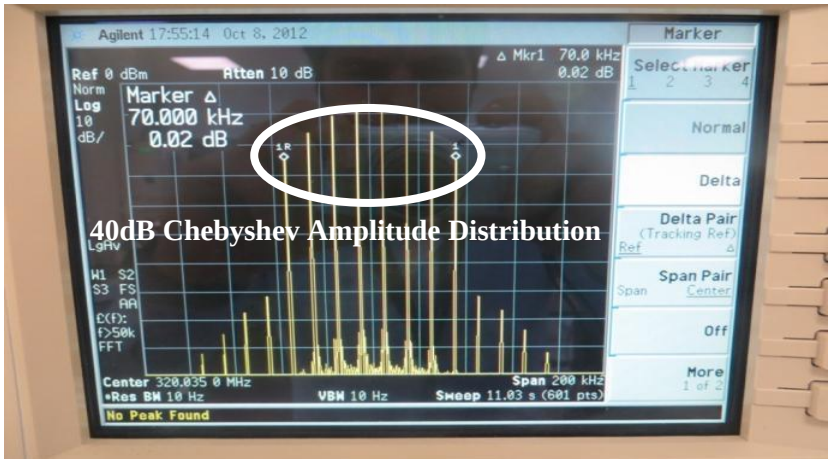

Figure 4.34: The output waveform of beam-former on the SA screen

CHAPTER 5

CONCLUSION AND FUTURE WORKS

This thesis presents a research on the theory and design of FDA for beam scanning and steering applications.

The frequency diverse array concept provides a new approach to hardware design for beam scanning and control. A frequency shift is only applied across the array elements in the simple FDA concept. This results in a periodically scanning beam without mechanical rotation or electronic phase shifters. This feature of the FDA may result in an affordable beam scanning option. Actually the T/R (transmit/receive) module takes a significant part of the whole cost of a conventional phased array. Moreover, the FDA offers more flexible beam control with finer steering angle resolution, since the time to transmit the pulse can be chosen randomly and consecutively, while phase shifters can only provide limited phase resolution.

Firstly, the theory of the FDA is developed by deriving the array factor and analyzing its characteristics. The periodicity of FDA's array factor with respect to time and distance, together with the relationship between scanning period and frequency shift, is mathematically verified.

The implementation of FDA is also considered. In this thesis the DDS frequency synthesis technique is introduced as an effective approach of generating the desired frequency diverse signals. The DDS based FDA beam-former network is designed with basic design considerations and guidelines. It is able to produce a frequency sinusoidal waveform at frequencies up to 400 MHz. By using this hardware, a variety of measurements are conducted to compare the theory and the real life results. The results are found to be compatible with the theory. Since the

CW-FDA has a periodically scanning beam and is not suitable for beam-steering applications, the remaining task is to measure the radiation pattern of the pulsed FDA. Due to time and budget limitation, this has not been performed in this thesis. Thus, the future work is to design and fabricate up-converters and antennas for DDS based FDA beam-former network. Then radiation patterns of pulses transmitted at different times can be measured.

REFERENCES

[1] H. E. Shanks, "A new technique for electronic scanning," *IRE Trans. on Antennas and Propagation,* vol. 9, pp.162-166, March 1961.

[2] T. Eker, "A Conceptual Evaluation OF Frequency Diverse Arrays and Novel Utilization OF LFMCW" Ph.D. thesis, The Graduate School of Natural and Applied Sciences of Middle East Technical University, September 2011.

[3] J. Huang, "Frequency Diversity Array: Theory and Design," Ph.D. thesis, University College London, Bloomsbury, London, UK, September 2010.

[4] W. L. Stutzman and G. A. Thiele, *Antenna Theory and Design*, 2nd ed. New York: John Wiley & Sons, 1998, pp. 107–109.

[5] J. Frank, "Bandwidth criteria for phased array antennas", in Phased Array Antennas, A.A. Oliner & G.H. Knittel, Artech House, pp. 243-253, 1972.

[6] J.S. Ajoika & J.L. McFarland, "Beam Forming Feeds", Chap. 19 of Antenna Handbook: Theory, Applications, and Design, Y.T. Lo and S.W. Lee (eds.), Van Nostrand, pp. 19-7 – 19-8, 1988.

[7] R. Tang, "Survey of Time Delay Beam Steering Techniques", in Phased Array Antennas, A.A. Oliner & G.H. Knittel, Artech House, pp. 254-260, 1972.

[8] W.B. Adams, "The broad-band signal response of a phase-steered linear receiving array", *Proc. IEEE*, vol. 52, issue 1, p. 106, Jan 1964.

[9] A.K. Agrawai, E. L. Williamson, J.G. Ferrante, “Design criteria for wideband active phased array antennas”, *1997 Digest Ant. Prop. Soc. Intl. Symp*., vol. 2, pp. 714-717, 13-18 July 1997.

[10] F. T. Ulaby, Fundamentals of Applied Electromagnetics, 5th ed. New Jersey: Pearson Prentice Hall, 2007, pp. 403–416.

[11] A. Aytun, “Frequency Diverse Array Radar” Ms.C thesis, Naval Postgraduate School, Monterey, California, USA, September 2010.

[12] M. I. Skolnik, Radar Handbook, 2nd ed. New York: McGraw-Hill, 1990.

[13] P. Antonik, “An investigation of a frequency diverse array,” Ph.D. thesis, University College London, Bloomsbury, London, UK, 2009.

[14] Antonik, P., Wicks, Michael C., Griffiths Hugh D., Baker Cristopher J., “Frequency Diverse Array Radars” Proc. 2006 IEEE Radar Conference, Verona NY, April 2006.

[15] Secmen M., Demir S., Hizal A., and Eker T., Frequency Diverse Array Antenna with Periodic Time Modulated Pattern in Range and Angle”. Proc. IEEE Radar Conference, pp. 427-430, April 2007.

[16] T. Eker, S. Demir, A. Hizal, "Exploitation of Linear Frequency Modulated Continuous Waveform (LFMCW) for Frequency Diverse Arrays", IEEE Trans. on Antennas and Propagation, vol. 61, no. 7, July 2013, pp 3546-3553.

[17] Cetintepe, Cagri, and Simsek Demir. "Multipath characteristics of frequency diverse arrays over a ground plane." (2014): 1-1.

[18] Cetintepe, Cagri, and Simsek Demir. "Examination of target RCS characteristics in FDA radars." Antennas and Propagation Society International Symposium (APSURSI), 2014 IEEE. IEEE, 2014.

[19] National Instruments Inc. "Understanding Direct Digital Synthesis (DDS)", http://www.ni.com/white-paper/5516/en/. [Last accessed on 25.02.2015]

[20] Analog Devices Inc., "1 GSPS, 14-Bit, 3.3 V CMOS Direct Digital Synthesizer", AD9910, http://www.analog.com/media/en/technical-documentation/data-sheets/AD9910.pdf. [Last accessed on 25.02.2015]

[21] Analog Devices Inc., "Fundamentals of Direct Digital Synthesis (DDS)", http://www.analog.com/media/en/training-seminars/tutorials/MT-085.pdf. [Last accessed on 25.02.2015]